M, et al. Comparison of multi-lineage cells from human adipose tissue and bone marrow. *Cells Tissues Organs* 2003; **174:** 101–109.
10. Kinnaird T, Stabile E, Burnett MS, Lee CW, Barr S, Fuchs S, et al. Marrow-derived stromal cells express genes encoding a broad spectrum of arteriogenic cytokines and promote in vitro and in vivo arteriogenesis through paracrine mechanisms. *Circ Res* 2004; **94:** 678–685.
11. Zuk PA, Zhu M, Mizuno H, Huang J, Futrell JW, Katz AJ, et al. Multilineage cells from human adipose tissue: Implications for cell-based therapies. *Tissue Eng* 2001; **7:** 211–228.
12. Miyahara Y, Nagaya N, Kataoka M, Yanagawa B, Tanaka K, Hao H, et al. Monolayered mesenchymal stem cells repair scarred myocardium after myocardial infarction. *Nature Med* 2006; **12:** 459–465.
13. Moon MH, Kim SY, Kim YJ, Kim SJ, Lee JB, Bae YC, et al. Human adipose tissue-derived mesenchymal stem cells improve postnatal neovascularization in a mouse model of hindlimb ischemia. *Cell Physiol Biochem* 2006; **17:** 279–290.
14. Gronthos S, Franklin DM, Leddy HA, Robey PG, Storms RW, Gimble JM. Surface protein characterization of human adipose tissue-derived stromal cells. *J Cell Physiol* 2001; **189:** 54–63.
15. Wakitani S, Saito T, Caplan AI. Myogenic cells derived from rat bone marrow mesenchymal stem cells exposed to 5-azacytidine. *Muscle Nerve* 1995; **18:** 1417–1426.
16. Solchaga LA, Penick K, Porter JD, Goldberg VM, Caplan AI, Welter JF. FGF-2 enhances the mitotic and chondrogenic potentials of human adult bone marrow-derived mesenchymal stem cells. *J Cell Physiol* 2005; **203:** 398–409.
17. Ohnishi S, Yasuda T, Kitamura S, Nagaya N. Effect of hypoxia on gene expression of bone marrow-derived mesenchymal stem cells and mononuclear cells. *Stem Cells* 2007; **25:** 1166–1177.
18. Hayashi O, Katsube Y, Hirose M, Ohgushi H, Ito H. Comparison of osteogenic ability of rat mesenchymal stem cells from bone marrow, periosteum, and adipose tissue. *Calcif Tissue Int* 2008; **82:** 238–247.
19. Lee RH, Kim B, Choi I, Kim H, Choi HS, Suh K, et al. Characterization and expression analysis of mesenchymal stem cells from human bone marrow and adipose tissue. *Cell Physiol Biochem* 2004; **14:** 311–324.
20. Zhu W, Shiojima I, Ito Y, Li Z, Ikeda H, Yoshida M, et al. IGFBP-4 is an inhibitor of canonical Wnt signalling required for cardiogenesis. *Nature* 2008; **454:** 345–349.
21. Boni A, Urbanek K, Nascimbene A, Hosoda T, Zheng H, Delucchi F, et al. Notch1 regulates the fate of cardiac progenitor cells. *Proc Natl Acad Sci USA* 2008; **105:** 15529–15534.
22. Tang XL, Rokosh DG, Guo Y, Bolli R. Cardiac progenitor cells and bone marrow-derived very small embryonic-like stem cells for cardiac repair after myocardial infarction. *Circ J* 2010; **74:** 390–404.
23. Hosoda T, Kajstura J, Leri A, Anversa P. Mechanisms of myocardial regeneration. *Circ J* 2010; **74:** 13–17.
24. Tsubokawa T, Yagi K, Nakanishi C, Zuka M, Nohara A, Ino H, et al. Impact of anti-apoptotic and -oxidative effects of bone marrow mesenchymal stem cells with transient overexpression of heme oxygenase-1 on myocardial ischemia. *Am J Physiol* 2010; **298:** 1320–1329.
25. Choi YS, Dusting GJ, Stubbs S, Arunothayaraj S, Han XL, Collas P, et al. Differentiation of human adipose-derived stem cells into beating cardiomyocytes. *J Cell Mol Med* 2010; **14:** 878–889.
26. Iwase T, Nagaya N, Fujii T, Itoh T, Murakami S, Matsumoto T, et al. Comparison of angiogenic potency between mesenchymal stem cells and mononuclear cells in a rat model of hindlimb ischemia. *Cardiovasc Res* 2005; **66:** 543–551.
27. Kinnaird T, Stabile E, Burnett MS, Epstein SE. Bone-marrow-derived cells for enhancing collateral development: Mechanisms, animal data, and initial clinical experiences. *Circ Res* 2004; **95:** 354–363.
28. Tang J, Wang J, Zheng F, Kong X, Guo L, Yang J, et al. Combination of chemokine and angiogenic factor genes and mesenchymal stem cells could enhance angiogenesis and improve cardiac function after acute myocardial infarction in rats. *Mol Cell Biochem* 2010; **339:** 107–118.
29. Nakanishi C, Yamagishi M, Yamahara K, Hagino I, Mori H, Sawa Y, et al. Activation of cardiac progenitor cells through paracrine effects of mesenchymal stem cells. *Biochem Biophys Res Commun* 2008; **374:** 11–16.
30. Hatzistergos KE, Quevedo H, Oskouei BN, Hu Q, Feigenbaum GS, Margitich IS, et al. Bone marrow mesenchymal stem cells stimulate cardiac stem cell proliferation and differentiation. *Circ Res* 2010; **107:** 913–922.
31. Rota M, Padin-Iruegas ME, Misao Y, De Angelis A, Maestroni S, Ferreira-Martins J, et al. Local activation or implantation of cardiac progenitor cells rescues scarred infarcted myocardium improving cardiac function. *Circ Res* 2008; **103:** 107–116.
32. Bhang SH, Cho SW, Lim JM, Kang JM, Lee TJ, Yang HS, et al. Locally delivered growth factor enhances the angiogenic efficacy of adipose-derived stromal cells transplanted to ischemic limbs. *Stem Cells* 2009; **27:** 1976–1986.
33. Wilson A, Shehadeh LA, Yu H, Webster KA. Age-related molecular genetic changes of murine bone marrow mesenchymal stem cells. *BMC Genomics* 2010; **229:** 7–11.

The Journal of International Medical Research
2011; 39: 549 – 557

Impact of Severe Coronary Disease Associated or Not Associated with Diabetes Mellitus on Outcome of Interventional Treatment Using Stents: Results from HERZ (Heart Research Group of Kanazawa) Analyses

K Uchiyama, H Ino, K Hayashi, K Fujioka, S Takabatake, J Yokawa, M Namura, S Mizuno, R Tatami, H Kanaya, Y Nitta, I Michishita, H Hirase, K Ueda, T Aoyama, K Okeie, T Haraki, K Mori, T Araki, M Minamoto, H Oiwake, T Konno, K Sakata, M Kawashiri and M Yamagishi; on behalf of the Heart Research Group of Kanazawa (HERZ)

Division of Cardiovascular Medicine, Kanazawa University Graduate School of Medicine, Kanazawa, Japan

Percutaneous coronary intervention (PCI) using a drug-eluting stent (DES) leads to less re-stenosis than PCI using a bare metal stent (BMS), however there is still controversy whether use of a DES for severe coronary disease leads to an acceptable outcome in patients with diabetes mellitus (DM). In this study 8159 lesions were treated in 6739 patients (mean age 68.9 years) with coronary artery disease. Use of a DES significantly decreased the re-stenosis rate compared with BMS in both DM (9.6% versus 21.3%) and non-DM (9.5% versus 17.1%) patients. The re-stenosis rate was significantly higher in DM than in non-DM patients in the BMS group but not in the DES group. There was no statistically significant difference in event-free survival after stenting of patients with left main coronary artery (LMCA) disease between the BMS and DES groups. It was concluded that, compared with BMS, DES reduced re-stenosis in patients with DM, however, we advise careful treatment after using DES for severe coronary disease, including LMCA lesions, in patients with DM.

KEY WORDS: Percutaneous coronary intervention; Drug-eluting stent; Bare metal stent; Coronary artery disease; Left main coronary artery disease; Diabetes mellitus; Major adverse cardiovascular events; Clinical outcome

Part of this work was presented at the 74th Annual Scientific Meeting of the Japanese Circulation Society, 5 – 7 March 2010, Kyoto, Japan.

Journal of Cardiology (2011) **57**, 89–94

available at www.sciencedirect.com

ScienceDirect

journal homepage: www.elsevier.com/locate/jjcc

Original article

Impact of reduced left atrial functions on diagnosis of paroxysmal atrial fibrillation: Results from analysis of time-left atrial volume curve determined by two-dimensional speckle tracking

Mika Mori (MD)[a], Hideaki Kanzaki (MD)[b], Makoto Amaki (MD)[b], Takahiro Ohara (MD)[b], Takuya Hasegawa (MD)[b], Hiroyuki Takahama (MD)[b], Kazuhiko Hashimura (MD)[b], Tetsuo Konno (MD)[a], Kenshi Hayashi (MD)[a], Masakazu Yamagishi (MD, FJCC)[a,*], Masafumi Kitakaze (MD, FJCC)[b]

[a] *Division of Cardiovascular Medicine, Kanazawa University Graduate School of Medicine, 13-1 Takara-machi, Kanazawa, 920-8641 Ishikawa, Japan*
[b] *Division of Heart Failure, Cardiovascular Medicine, National Cerebral and Cardiovascular Center, Suita, Osaka, Japan*

Received 4 August 2010; accepted 11 August 2010
Available online 15 October 2010

KEYWORDS
Atrial fibrillation;
Echocardiography;
Speckle tracking method;
Reservoir function;
Booster function

Summary
Background: Atrial fibrillation is commonly associated with impaired reservoir and booster functions of the left atrium (LA). Recent advances in two-dimensional speckle tracking technique (2DST) enabled automatic analysis of the time-LA volume curve representing these functions. Our objective was to evaluate LA function in patients with or without paroxysmal atrial fibrillation (PAF) using 2DST.
Methods: We studied 111 patients (68 men, age 62 ± 16 years) with (n = 53) or without (n = 58) PAF. After constructing time-LA volume curves from the apical four and two chamber views (iE33, Philips with QLAB 6.0, Philips Medical Systems, Bothell, WA, USA), maximal LA volume (LAVmax), preatrial contraction LA volume (LAVpreA), and minimum LA volume (LAVmin) were obtained. Then, LA reservoir volume (ARV = LAVmax − LAVmin) and active emptying volume (AEV = LAVpreA − LAVmin) were calculated to determine ARV/LAVmax as reservoir function and AEV/LAVpreA as booster pump function.

* Corresponding author. Tel.: +81 6 76 265 2259; fax: +81 76 234 4210.
E-mail address: myamagi@med.kanazawa-u.ac.jp (M. Yamagishi).

0914-5087/$ – see front matter
doi:10.1016/j.jjcc.2010.08.006

Results: PAF was associated with greater LAVmax than that in controls (80 ± 21 ml versus 65 ± 16 ml, $p < 0.001$) and with reduced reservoir and booster functions (ARV/LAVmax 46 ± 9% versus 52 ± 7%; AEV/LAVpreA 29 ± 10% versus 36 ± 6%, $p < 0.001$). Multivariate logistic analysis demonstrated that ARV/LAVmax and AEV/LAVpreA were closely associated with the existence of PAF.

Conclusion: These results demonstrate that the present 2DST enables determining LA reservoir and booster functions, providing insights into the diagnosis of PAF.

Introduction

It is well established that cardiogenic embolism could suddenly occlude the cerebral artery without the development of collateral circulation, thus resulting in large infarction associated with severe paralysis and/or consciousness disturbance. Actually, atrial fibrillation (AF) is the independent risk factor for cardiogenic stroke and relative risk increases up to 5 times in comparison with cases without AF [1]. There exists a strong correlation between left atrial (LA) volume and occurrence of AF [2], and an enlarged LA could be a predictive factor for the occurrence of stroke even without the evidence of AF [3]. This suggests that the diagnosis of possible occurrence of AF at the time of sinus rhythm is important for the prevention of cardiogenic stroke when considering that paroxysmal AF (PAF) has the same impact on the occurrence of stroke as persistent or chronic AF [4].

LA mechanical functions consist of three components at different stages of the cardiac cycle: active and passive LA enlargement, as a reservoir, associated with pulmonary inflow at the time of left ventricular systole to isovolumetric relaxation, conduit function during early ventricular diastole, and active systole to transfer blood, as a booster, during late ventricular diastole [5]. Although AF is a situation in which LA booster pump function is lost, this booster function as well as reservoir function could be impaired even in PAF [6–8].

Although three-dimensional echocardiography [9] and acoustic quantification (AQ) [10,11] have been used for the evaluation of these LA functions, they were somewhat complicated to obtain reliable results. Recent advances in two-dimensional speckle tracking technique (2DST) enabled analyzing time-LA volume curve [12]. In the present study, using 2DST we attempted to evaluate LA function in patients with or without PAF examining possible indices to diagnose PAF.

Methods

Study subjects

We studied a total of 111 patients (68 men, age 62 ± 16 years) including 53 patients with PAF which was documented by electrocardiogram (ECG) including conventional, ambulatory, and remote monitoring systems, and 58 patients who did not exhibit any cardiac abnormalities with sinus rhythm as controls. Exclusion criteria included the presence of significant valvular disease, intracardiac shunting, left ventricular (LV) systolic dysfunction defined as LV ejection fraction (EF) < 50%, hyperthyroidism, primary pulmonary hypertension, and respiratory disease. We also excluded patients who showed inadequate echocardiographic images. All the research protocols were approved by ethical committee and informed consent was obtained from all patients.

Patients' characteristics in the present study included age, sex, height, body weight, systolic blood pressure, diastolic blood pressure, heart rate, absence or presence of hypertension, diabetes mellitus, and dyslipidemia. Current drug treatments were also recorded. Hypertension was defined as systolic blood pressure ≥140 mm Hg and/or diastolic blood pressure ≥90 mm Hg. We also defined hypertension if patients already had anti-hypertensive medication. Diabetes mellitus was defined when diabetic patterns such as fasting plasma glucose levels ≥126 mg/dl, 2-h plasma glucose levels by 75 g oral glucose tolerance test ≥200 mg/dl, or casual plasma glucose levels ≥200 mg/dl were observed on at least two occasions. Patients who exhibited diabetic pattern at least once and diabetic symptoms or retinopathy or HbA1c ≥6.5% were also defined as having diabetes mellitus. Dyslipidemia was defined as low-density lipoprotein cholesterol ≥140 mg/dl and/or high-density lipoprotein cholesterol <40 mg/dl or triglyceride ≥150 mg/dl.

Echocardiography

All echocardiographic examinations were performed using an iE33 system and an S5-1 broadband phased array transducer (Philips Medical Systems, Bothell, WA, USA). At first, LA dimension was determined by M-mode from the parasternal long-axis view. Then, thickness of interventricular septum and posterior wall, LV end-diastolic and end-systolic dimensions, and LVEF were determined in accordance with the guideline of the American Society of Echocardiography [13].

Using pulsed Doppler method, transmitral flow velocity such as *E* and *A* waves, and deceleration time of *E* wave (E-DcT) were measured. Finally, from the apical four chamber view, the average of peak early and late diastolic mitral annular velocity (e' and a') between medial and lateral sides was determined by pulsed tissue Doppler method. E/e' was then calculated as an index of LV end-diastolic pressure.

Analysis of time-left atrial volume curve

We analyzed echocardiographic data using commercially available QLAB 6.0 software (Philips Medical Systems). Briefly, when we set three points at the septal and lateral sides of mitral annulus and roof of LA in the apical four chamber view at LV end-diastole defined as R wave on the ECG, software automatically drew a region of interest (ROI) like

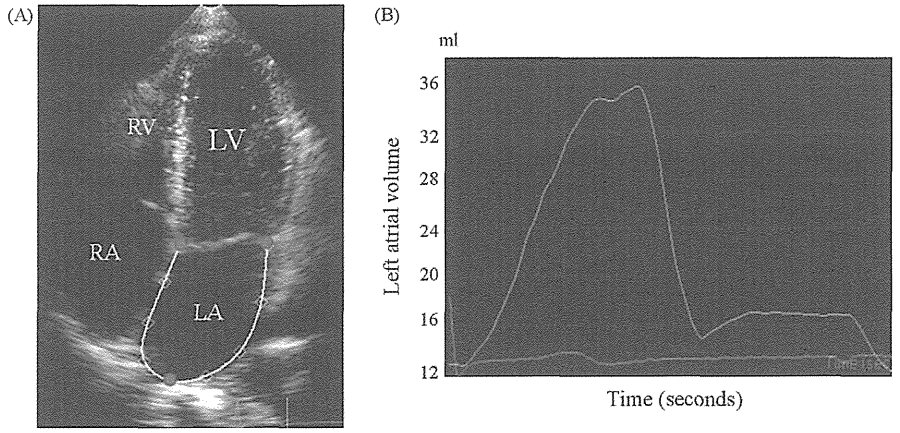

Figure 1 (A) Two-dimensional speckle tracking in the left atrial wall. Red circles represent initially set regions of interest (ROIs). White squares represent ROIs which are automatically added. White lines represent complementary lines between each ROI. (B) Representative left atrial volume curve during a cardiac cycle. LA, left atrium; LV, left ventricle; RA, right atrium; RV, right ventricle. (For interpretation of the references to color in this figure legend, the reader is referred to the web version of the article.)

a horseshoe shape at the inner side of LA wall, the septal and lateral sides of mitral annulus, and the top of LA. In the present study, we changed the setup of the number of points to drag and modify the shape of ROI to three at each wall (total 9 points). After manually adjusting the ROI, LA volume was calculated by Simpson's rule using spline interpolation frame by frame throughout the cardiac cycle to derive a time-LA volume curve (Fig. 1). Then, a time-LA volume curve was also obtained from the apical two-chamber view as well.

Three types of LA volume were determined: maximal LA volume (LAVmax) at the LV end-systolic phase just before mitral valve opening, preatrial contraction LA volume (LAVpreA) at the beginning of P-wave on the ECG, and minimal LA volume (LAVmin) at the LV end-diastolic phase just after mitral valve closure (Fig. 2). We calculated LA reservoir volume (ARV = LAVmax − LAVmin) and active emptying volume (AEV = LAVpreA − LAVmin) and defined ARV/LAVmax as a reservoir index and AEV/LAVpreA as a booster pump index according to the published reports [5,11].

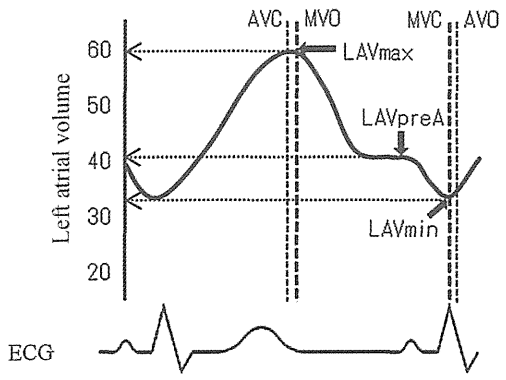

Figure 2 Schematic representations of time-left atrial volume curve and measurement of left atrial volume. AVC, aortic valve closure; AVO, aortic valve opening; ECG, electrocardiogram; LAVmax, maximum left atrial volume; LAVmin, minimum left atrial volume; LAVpreA, preatrial contraction left atrial volume; MVC, mitral valve closure; MVO, mitral valve opening.

Statistical analysis

Data are shown as mean ± SD. An analysis of variance (ANOVA) was performed to test for statistically significant differences between two unpaired mean values, and categorical data and percentage frequencies were analyzed by the chi-square test. PAF-associated factors were examined by multivariate logistic analysis. We used SPSS 16.0J for Windows for analysis (SPSS Inc, Chicago, IL, USA). Statistical significance was considered when $p < 0.05$.

Twenty subjects were randomly selected and analyzed to assess reproducibility. The inter- and intraobserver variability was 5.7 ± 3.2% and 6.2 ± 3.9% for LAVmax, 7.6 ± 5.0% and 5.8 ± 4.9% for LAVpreA, 7.0 ± 4.6% and 7.7 ± 3.3% for LAVmin.

Results

Patients' backgrounds

Age and systolic and diastolic blood pressures were higher in PAF than those in controls, although heart rate was lower in controls. There were no differences in sex and BMI between two groups. Also there were no differences in incidence of hypertension, diabetes, and dyslipidemia. Although the use of angiotensin-converting enzyme inhibitors and/or angiotensin II receptor blockers was not different in both groups, the use of β-blockers was greater in PAF than that in non-PAF (Table 1).

In echocardiographic parameters, LA dimension and *E* wave velocity were greater in PAF, although E-DcT was shorter in PAF. E/e' was greater in PAF because of significantly decreased e' and increased *E*. There were no

Table 1 Patients' background.

Parameters	Control group ($n = 58$)	PAF group ($n = 53$)	p-value
Age, years	58 ± 17	66 ± 13	0.002
Male, %	57	66	NS
Body mass index, kg/m^2	23 ± 2.8	23 ± 2.4	NS
Systolic blood pressure, mm Hg	132 ± 18	139 ± 18	0.023
Diastolic blood pressure, mm Hg	76 ± 12	80 ± 10	0.026
Heart rate, beats/min	65 ± 10	60 ± 8	0.013
Hypertension, %	57	58	NS
Diabetes mellitus, %	16	10	NS
Dyslipidemia, %	21	16	NS
Drug treatment			
ACEI or ARB, %	11	9	NS
Beta-blocker, %	3	12	0.016

Data are mean ± SD.
ACEI, angiotensin-converting enzyme inhibitor; ARB, angiotensin II receptor blocker; PAF, paroxysmal atrial fibrillation.

significant differences in LV dimensions, LV fractional shortening, LV wall thickness, *A* wave velocity, *E*/*A* and *a*′ between the two groups (Table 2).

Left atrial volume and indices of left atrial function

All data regarding LA volume and functional indices are summarized in Table 3. LAVmax, LAVpreA, and LAVmin were greater in PAF than those in controls ($p < 0.05$). As for LA functions, both ARV/LAVmax as the index for reservoir function and AEV/LAVpreA as the index for booster pump function were lower in PAF in comparison with those in controls ($p < 0.05$).

Determining factors for PAF

We determined the diagnostic value of the LA volume and function in predicting PAF using logistic analysis. After adjusting for age, sex, and presence or absence of hypertension, increases in LAVmax, and decreases in ARV/LAVmax and AEV/LAVpreA were associated with the existence of PAF (Table 4).

Table 2 Echocardiographic parameters.

Parameters	Control group	PAF group	p-value
LA dimension, mm	37 ± 5	40 ± 6	0.002
LVDd, mm	45 ± 3	47 ± 5	NS
LVDs, mm	28 ± 3	29 ± 4	NS
LVFS, %	37 ± 6	38 ± 5	NS
IVS, mm	9 ± 1	9 ± 1	NS
PW, mm	9 ± 1	9 ± 1	NS
E velocity, cm/s	63 ± 18	71 ± 16	0.017
A velocity, cm/s	67 ± 20	73 ± 20	NS
E/*A*	1.1 ± 0.6	1.1 ± 0.5	NS
E-DcT, ms	230 ± 60	209 ± 44	0.037
e′, cm/s	8.4 ± 3.5	7.1 ± 2.0	0.017
a′, cm/s	9.8 ± 1.6	8.9 ± 2.2	NS
E/*e*′	8.3 ± 3.4	10.5 ± 3.6	0.001

Data are mean ± SD. *a*′, peak late diastolic mitral annular velocity; *e*′, peak early diastolic mitral annular velocity; E-DcT, *E* wave deceleration time; IVS, interventricular wall thickness; LA, left atrium; LVDd, left ventricular end-diastolic dimension; LVDs, left ventricular end-systolic dimension; LVFS, left ventricular fractional shortening; PAF, paroxysmal atrial fibrillation; PW, posterior wall thickness.

Table 3 Left atrial volume and functional indices by two-dimensional speckle tracking method.

Parameters	Control group	PAF group	p-value
LAVmax, ml	65 ± 16	80 ± 21	0.002
LAVpreA, ml	49 ± 15	61 ± 19	0.037
LAVmin, ml	31 ± 10	44 ± 16	0.004
ARV/LAVmax, %	52.2 ± 7.1	46.3 ± 9.3	0.001
AEV/LAVpreA, %	35.6 ± 5.8	28.6 ± 9.6	0.001

Data are mean ± SD.
AEV, active emptying volume = LAVpreA − LAVmin; ARV, atrial reservoir volume = LAVmax − LAVmin; LAVmax, maximum left atrial volume; LAVpreA, preatrial contraction left atrial volume; LAVmin, minimum left atrial volume; PAF, paroxysmal atrial fibrillation.

Table 4 Adjusted odds ratio for paroxysmal atrial fibrillation.

	Odds ratio (95%CI)	p-value
LAVmax, ml	1.534 (1.186–1.983) (/10 ml increase)	0.001
LAVmax/BSA, ml/m^2	2.135 (1.335–3.414) (10 ml/m^2 increase)	0.002
ARV/LAVmax, %	1.457 (1.117–1.900) (5% decline)	0.005
AEV/LAVpreA, %	1.835 (1.334–2.523) (5% decline)	<0.001

Data are mean ± SD.
AEV, active emptying volume = LAVpreA − LAVmin; ARV, atrial reservoir volume = LAVmax − LAVmin; BSA, body surface area; CI, confidence interval; LAVmax, maximal left atrial volume; LAVpreA, preatrial contraction left atrial volume.

Discussion

Occurrence of paroxysmal atrial fibrillation and left atrial function

Enlargement of LA is known to be related to aging, hypertension, and LV diastolic dysfunction, and is an independent factor for occurrence of AF [14–17]. In the present study, LAVmax was found to be an independently associated factor for paroxysmal AF even after adjusting for other factors such as aging, sex, and presence of hypertension. On the other hand, enlargement of LA reflects the duration of AF periods, because AF itself can enhance LA remodeling [17]. In addition to LAVmax, LAVpreA and LAVmin were found to be greater in PAF than those in controls. Fatema et al. [18] reported that not only LAVmax but also LAVmin were independent predicting factors for AF, and, under these conditions, LAVmin might be better than LAVmax in terms of predicting value for AF. However, as pointed out in a previous [18] and in our study, reproducibility for measurement of LAVmin was found not enough to use for clinical practice.

LA reservoir function is considered as a combination of active LA dilation and passive dilation due to declining of mitral annulus associated with LV contraction. Abhayaratna et al. [19] demonstrated that the probability of occurrence of AF would increase by 9 times in patients with LAVmax/BSA $\geq$38 ml/m^2 and ARV/LAVmax $\leq$49% in comparison with patients with LAVmax/BSA <38 ml/m^2 and ARV/LAVmax >49%. This suggests that in addition to LA volume, evaluation of LA function should be done to predict the occurrence of AF.

LA reservoir function can represent LA diastolic function and can be evaluated by the strain-rate imaging method. Wang et al. [7] reported that hypertensive patients with PAF exhibited lower LA strain rate than those without PAF, suggesting that LA reservoir function may reflect the progression of atrial remodeling because the recurrence rate of AF after catheter ablation was higher in patients with low strain rates of left ventricle and atrium [20]. The present ARV/LAVmax actually represented LA reservoir function and was reduced in PAF, suggesting that this reflected the impaired reservoir function. From the time-LA volume curve obtained by 2DST, we can obtain first derivation curve which also represents the strain rate of the whole left atrium. Unfortunately, it was somewhat difficult to obtain reliable data regarding peak value of this index from the present study because of the presence of artifact due to noise. However, it will be possible to overcome these difficulties if adequate frame rates and adequate noise filters are chosen.

LA booster pump function can increase in accordance with increase in LA preload until disruption of Frank–Starling law and contribute to maintaining cardiac output [5,21]. However, this function may decrease in accordance with progression of LA remodeling associated with AF [22]. Cui et al. [8] reported that AEV/LAVpreA which was determined by AQ method was significantly lower in PAF with hypertension than that without PAF. As for other indices for assessment of LA function, *A* wave velocity [23] and tissue Doppler-derived *a'* [24] were used. In the present study, there were significant differences in AEV/LAVpreA despite the absence of significant differences in *A* wave and *a'*, suggesting that AEV/LAVpresA determined by 2DST is more sensitive in the evaluation of LA remodeling in clinical settings.

Two-dimensional speckle tracking method

Previously, measurement of LA volume for time-LA volume curve analysis has been performed by the AQ method [10,11]. However, it is somewhat difficult to exclude the presence of pulmonary vein and/or LA appendage, thus resulting in inadequate quantification of LA volume, because automatic determination of blood-tissue border by the AQ method is performed within an oval ROI [25]. In contrast, in the 2DST method we can set an ROI freely and adjust it on looking at the situation of tracking. Therefore, one might speculate that measurement might be more accurate in 2DST than that in AQ.

Although LA volume determined by three-dimensional echocardiography coincided well with that determined by magnetic resonance imaging [9], this procedure requires some technical experience and time. We previously reported that LA volume measured by 2DST coincided well with that by real-time three-dimensional echocardiography [26]. Ogawa et al. [27] demonstrated that time to create time-LA volume curve by 2DST was much shorter than that by manual examination. Okamatsu et al. [12] studied 140 subjects by 2DST on LA reservoir and booster functions and demonstrated impaired reservoir and enhanced booster functions were observed in old people. This suggests the higher sensitivity of the present study to detect the LA reservoir and booster functions than previous methods in clinical settings, although we did not compare each methodology.

Study limitations

There remain several limitations in the present study. First, we examined patients without evidenced PAF as controls. However, we could not exclude the possibility that these controls might have an asymptomatic AF. Also it was difficult to determine the adequate cutoff value in each index because of the limited number of subjects. Second, the present study was not longitudinal but a transverse study and, thus, it is difficult to predict the occurrence of AF and/or thromboembolism. To complete this issue, additional follow-up study will be required to determine absolute value of these indices for predicting the occurrence of clinical events.

Conclusions

The present study demonstrates that using 2DST LA reservoir and booster functions in PAF are impaired in comparison with controls. We suggest that the indices obtained by the present method provide alternative objective findings for predicting possible occurrence of PAF.

Acknowledgments

A part of this work was presented at the 57th Annual Scientific Sessions, Japanese College of Cardiology, 2009, Sapporo, Japan.

References

[1] Wolf PA, Abbott RD, Kannel WB. Atrial fibrillation as an independent risk factor for stroke: the Framingham Study. Stroke 1991;22:983–8.

[2] Tsang TS, Barnes ME, Bailey KR, Leibson CL, Montgomery SC, Takemoto Y, Diamond PM, Marra MA, Gersh BJ, Wiebers DO, Petty GW, Seward JB. Left atrial volume: important risk marker of incident atrial fibrillation in 1655 older men and women. Mayo Clin Proc 2001;76:467–75.

[3] Barnes ME, Miyasaka Y, Seward JB, Gersh BJ, Rosales AG, Bailey KR, Petty GW, Wiebers DO, Tsang TS. Left atrial volume in the prediction of first ischemic stroke in an elderly cohort without atrial fibrillation. Mayo Clin Proc 2004;79:1008–14.

[4] Hohnloser SH, Pajitnev D, Pogue J, Healey JS, Pfeffer MA, Yusuf S, Connolly SJ, ACTIVE W Investigators. Incidence of stroke in paroxysmal versus sustained atrial fibrillation in patients taking oral anticoagulation or combined antiplatelet therapy: an ACTIVE W Substudy. J Am Coll Cardiol 2007;50:2156–61.

[5] Zhang G, Yasumura Y, Uematsu M, Nakatani S, Nagaya N, Miyatake K, Yamagishi M. Echocardiographic determination of left atrial function and its application for assessment of mitral flow velocity pattern. Int J Cardiol 1999;72:19–25.

[6] Barbier P, Alioto G, Guazzi MD. Left atrial function and ventricular filling in hypertensive patients with paroxysmal atrial fibrillation. J Am Coll Cardiol 1994;24:165–70.

[7] Wang Z, Tan H, Zhong M, Jiang G, Zhang Y, Zhang W. Strain rate imaging for noninvasive functional quantification of the left atrium in hypertensive patients with paroxysmal atrial fibrillation. Cardiology 2008;109:15–24.

[8] Cui Q, Wang H, Zhang W, Wang H, Sun X, Zhang Y, Yang H. Enhanced left atrial reservoir, increased conduit, and weakened booster pump function in hypertensive patients with paroxysmal atrial fibrillation. Hypertens Res 2008;31:395–400.

[9] Poutanen T, Ikonen A, Vainio P, Jokinen E, Tikanoja T. Left atrial volume assessed by transthoracic three dimensional echocardiography and magnetic resonance imaging: dynamic changes during the heart cycle in children. Heart 2000;83:537–42.

[10] Zhang GC, Tsukada T, Nakatani S, Uematsu M, Yasumura Y, Tanaka N, Masuda Y, Miyatake K, Yamagishi M. Comparison of automatic boundary detection and manual tracing technique in echocardiographic determination of left atrial volume. Jpn Circ J 1998;62:755–9.

[11] Spencer KT, Mor-Avi V, Gorcsan III J, DeMaria AN, Kimball TR, Monaghan MJ, Perez JE, Weinert L, Bednarz J, Edelman K, Kwan OL, Glascock B, Hancock J, Baumann C, Lang RM. Effects of aging on left atrial reservoir, conduit, and booster pump function: a multi-institution acoustic quantification study. Heart 2001;85:272–7.

[12] Okamatsu K, Takeuchi M, Nakai H, Nishikage T, Salgo IS, Husson S, Otsuji Y, Lang RM. Effects of aging on left atrial function assessed by two-dimensional speckle tracking echocardiography. J Am Soc Echocardiogr 2009;22:70–5.

[13] Lang RM, Bierig M, Devereux RB, Flachskampf FA, Foster E, Pellikka PA, Picard MH, Roman MJ, Seward J, Shanewise JS, Solomon SD, Spencer KT, Sutton MS, Stewart WJ. Recommendations for chamber quantification: a report from the American Society of Echocardiography's Guidelines and Standards Committee and the Chamber Quantification Writing Group, developed in conjunction with the European Association of Echocardiography, a branch of the European Society of Cardiology. J Am Soc Echocardiogr 2005;18:1440–63.

[14] Casaclang-Verzosa G, Gersh BJ, Tsang TS. Structural and functional remodeling of the left atrium: clinical and therapeutic implications for atrial fibrillation. J Am Coll Cardiol 2008;51:1–11.

[15] Psaty BM, Manolio TA, Kuller LH, Kronmal RA, Cushman M, Fried LP, White R, Furberg CD, Rautaharju PM. Incidence of and risk factors for atrial fibrillation in older adults. Circulation 1997;96:2455–61.

[16] Healey JS, Connolly SJ. Atrial fibrillation: hypertension as a causative agent, risk factor for complications, and potential therapeutic target. Am J Cardiol 2003;91:9G–14G.

[17] Thamilarasan M, Klein AL. Factors relating to left atrial enlargement in atrial fibrillation: ''chicken or the egg'' hypothesis. Am Heart J 1999;137:381–3.

[18] Fatema K, Barnes ME, Bailey KR, Abhayaratna WP, Cha S, Seward JB, Tsang TS. Minimum vs. maximum left atrial volume for prediction of first atrial fibrillation or flutter in an elderly cohort: a prospective study. Eur J Echocardiogr 2009;10: 282–6.

[19] Abhayaratna WP, Fatema K, Barnes ME, Seward JB, Gersh BJ, Bailey KR, Casaclang-Verzosa G, Tsang TS. Left atrial reservoir function as a potent marker for first atrial fibrillation or flutter in persons > or = 65 years of age. Am J Cardiol 2008;101:1626–9.

[20] Schneider C, Malisius R, Krause K, Lampe F, Bahlmann E, Boczor S, Antz M, Ernst S, Kuck KH. Strain rate imaging for functional quantification of the left atrium: atrial deformation predicts the maintenance of sinus rhythm after catheter ablation of atrial fibrillation. Eur Heart J 2008;29:1397–409.

[21] Anwar AM, Geleijnse ML, Soliman OI, Nemes A, ten Cate FJ. Left atrial Frank–Starling law assessed by real-time, three-dimensional echocardiographic left atrial volume changes. Heart 2007;93:1393–7.

[22] Toh N, Kanzaki H, Nakatani S, Ohara T, Kim J, Kusano KF, Hashimura K, Ohe T, Ito H, Kitakaze M. Left atrial volume combined with atrial pump function identifies hypertensive patients with a history of paroxysmal atrial fibrillation. Hypertension 2010;55:1150–6.

[23] Manning WJ, Silverman DI, Katz SE, Riley MF, Come PC, Doherty RM, Munson JT, Douglas PS. Impaired left atrial mechanical function after cardioversion: relation to the duration of atrial fibrillation. J Am Coll Cardiol 1994;23:1535–40.

[24] Nagueh SF, Sun H, Kopelen HA, Middleton KJ, Khoury DS. Hemodynamic determinants of the mitral annulus diastolic velocities by tissue Doppler. J Am Coll Cardiol 2001;37:278–85.

[25] Tsujita-Kuroda Y, Zhang G, Sumita Y, Hirooka K, Hanatani A, Nakatani S, Yasumura Y, Miyatake K, Yamagishi M. Validity and reproducibility of echocardiographic measurement of left ventricular ejection fraction by acoustic quantification with tissue harmonic imaging technique. J Am Soc Echocardiogr 2000;13:300–5.

[26] Mori M, Hasegawa T, Kanzaki H, Maeda M, Yoshida A, Watanabe M, Harada K, Takahama H, Amaki M, Ohara T, Hashimura K, Kitakaze M. Evaluation of left atrial function in paroxysmal atrial fibrillation: application of two-dimensional speckle tracking method for analysis of left atrial volume curve. J Cardiol 2009;4(Suppl. I):220.

[27] Ogawa K, Hozumi T, Sugioka K, Iwata S, Otsuka R, Takagi Y, Yoshitani H, Yoshiyama M, Yoshikawa J. Automated assessment of left atrial function from time-left atrial volume curves using a novel speckle tracking imaging method. J Am Soc Echocardiogr 2009;22:63–9.

Journal of Molecular and Cellular Cardiology 50 (2011) 50–57

Contents lists available at ScienceDirect

Journal of Molecular and Cellular Cardiology

journal homepage: www.elsevier.com/locate/yjmcc

Original article

A *KCR1* variant implicated in susceptibility to the long QT syndrome

Kenshi Hayashi [a,*], Noboru Fujino [a], Hidekazu Ino [a], Katsuharu Uchiyama [a], Kenji Sakata [a], Tetsuo Konno [a], Eiichi Masuta [a], Akira Funada [a], Yuichiro Sakamoto [a], Toshinari Tsubokawa [a], Akihiko Hodatsu [a], Toshihiko Yasuda [b], Honin Kanaya [b], Min Young Kim [c], Sabina Kupershmidt [c], Haruhiro Higashida [d], Masakazu Yamagishi [a]

[a] *Division of Cardiovascular Medicine, Kanazawa University Graduate School of Medical Science, Kanazawa, Ishikawa, Japan*
[b] *Ishikawa Prefectural Central Hospital, Kanazawa, Ishikawa, Japan*
[c] *Anesthesiology Research Division, Vanderbilt University, Nashville, TN, USA*
[d] *Department of Biophysical Genetics, Kanazawa University Graduate School of Medical Science, Kanazawa, Ishikawa, Japan*

ARTICLE INFO

Article history:
Received 12 January 2010
Received in revised form 2 October 2010
Accepted 5 October 2010
Available online 13 October 2010

Keywords:
Ion channels
Long-QT syndrome
Drugs
Electrophysiology
Hypokalemia

ABSTRACT

The acquired long QT syndrome (aLQTS) is frequently associated with extrinsic and intrinsic risk factors including therapeutic agents that inadvertently inhibit the KCNH2 K^+ channel that underlies the repolarizing I_{Kr} current in the heart. Previous reports demonstrated that K^+ channel regulator 1 (KCR1) diminishes KCNH2 drug sensitivity and may protect susceptible patients from developing aLQTS. Here, we describe a novel variant of *KCR1* (E33D) isolated from a patient with ventricular fibrillation and significant QT prolongation. We recorded the KCNH2 current (I_{KCNH2}) from CHO-K1 cells transfected with *KCNH2* plus wild type (WT) or mutant *KCR1* cDNA, using whole cell patch-clamp techniques and assessed the development of I_{KCNH2} inhibition in response to well-characterized KCNH2 inhibitors. Unlike *KCR1* WT, the E33D variant did not protect KCNH2 from the effects of class I antiarrhythmic drugs such as quinidine or class III antiarrhythmic drugs including dofetilide and sotalol. The remaining current of the KCNH2 WT + KCR1 E33D channel after 100 pulses in the presence of each drug was similar to that of KCNH2 alone. Simulated conditions of hypokalemia (1 mM $[K^+]_o$) produced no significant difference in the fraction of the current that was protected from dofetilide inhibition with KCR1 WT or E33D. The previously described α-glucosyltransferase activity of KCR1 was found to be compromised in KCR1 E33D in a yeast expression system. Our findings suggest that *KCR1* genetic variations that diminish the ability of KCR1 to protect KCNH2 from inhibition by commonly used therapeutic agents constitute a risk factor for the aLQTS.

1. Introduction

The long QT syndrome (LQTS) can be of the acquired form, which is characterized by pathogenic excessive prolongation of the QT interval, with risk for torsade de pointes (TdP) upon exposure to an environmental stressor [1]. A minority (less than 10%) of probands with the drug-induced acquired LQTS (aLQTS) are known to be affected by a subclinical congenital syndrome [1]. Thus, a subset of aLQTS patients carry mutations in *KCNQ1, KCNH2, KCNE1, KCNE2,* and *SCN5A* [2–6]. Among them, KCNH2 plays an important role in cardiac repolarization because KCNH2 channels conduct the rapid delayed rectifier K^+ current (I_{Kr}) which is an important component of phase 3 repolarization of cardiac muscle.

Multiple proteins are known to affect the function of KCNH2 in heterologous systems. MiRP1 encoded by *KCNE2* is thought to regulate KCNH2 in the human heart; MinK encoded by *KCNE1* may also modulate KCNH2 in vivo; 14-3-3ε binding to KCNH2 channels shifts the activation curve towards more hyperpolarized potentials; GM130, a Golgi-associated protein, interacts with KCNH2 as the channel is transported between the endoplasmic reticulum and the plasma membrane [7–10]. These proteins that influence KCNH2 function must also be considered candidates for arrhythmia causing genes. We previously identified a protein that accelerated the activation of rat EAG K^+ channels and called it K^+ channel regulator 1 (KCR1) [11]. We also found that KCR1 did not alter KCNH2 current (I_{KCNH2}) properties in heterologous systems, but that overexpression protected I_{KCNH2} from blockade by dofetilide, sotalol, or quinidine [12]. We subsequently demonstrated that in mammalian cells, the yeast α-glucosyltransferase, *ALG10*, which is the closest homolog of *KCR1*, also inhibited dofetilide blockade of I_{KCNH2} [13]. The I447V variant of *KCR1* occurred in 1.1% of patients with drug-induced TdP, compared with 7% of controls, suggesting that the presence of valine

* Corresponding author. Division of Cardiovascular Medicine, Kanazawa University Graduate School of Medical Science, 13-1, Takara-machi, Kanazawa , Ishikawa 920-8640, Japan. Fax: +81 76 234 4251.
E-mail address: kenshi@med.kanazawa-u.ac.jp (K. Hayashi).

0022-2828/$ – see front matter © 2010 Elsevier Ltd. All rights reserved.
doi:10.1016/j.yjmcc.2010.10.007

in this position may exert a protective effect [14]. In a heterologous expression system, the I447V variant was more effective at protecting KCNH2 against dofetilide inhibition than wild type (WT) KCR1 [14]. Thus, we concluded that KCR1 can modulate the risk of drug-induced cardiac arrhythmias. In the present study, we identified a *KCR1* genetic variant (E33D) in a patient who suffered ventricular fibrillation and QT prolongation, and characterized electrophysiological alterations and changes in drug sensitivity of this variant. We also evaluated the enzymatic α-glycosyltransferase function of this variant in a yeast expression system.

2. Methods

2.1. Study population and mutation analysis

We evaluated 14 patients (8 females and 6 males, mean age 66 ± 24 years) with aLQTS, which was defined as a prolonged corrected QT interval (QTc > 550 ms) and an episode of TdP or ventricular fibrillation induced by drugs or associated with other underlying conditions. To identify gene mutations, we performed genetic analysis after obtaining written informed consent from the patients in accordance with the guidelines of the Bioethical Committee on Medical Research of Kanazawa University. Genomic DNA was purified from white blood cells and amplified using a standard polymerase chain reaction (PCR) method. Single-strand conformational polymorphism (SSCP) analysis of the amplified DNA was performed to screen for mutations in all exons of *KCR1*, *KCNQ1*, *KCNH2*, *SCN5A*, *KCNE1*, and *KCNE2*. Normal and aberrant mutant DNA strands identified in SSCP analysis were isolated and sequenced using an ABI PRISM 310 Genetic Analyzer (PE Applied Biosystems, Foster City, CA).

2.2. Plasmid constructs

The *KCNH2* cDNA was subcloned into the mammalian expression vector pSI (Promega, Madison, WI), as described previously [15]. The human *KCR1* cDNA was subcloned into the pCGI vector for bicistronic expression with enhanced green fluorescent protein (GFP). For expression in yeast, *ALG10* and *KCR1* WT were subcloned into the pGPD426 yeast shuttle vector that allows for selection on uracil-deficient media, as described previously [13,16]. The *KCR1* E33D cDNA was constructed by an overlap extension strategy [17]. The sequence of the *KCR1* E33D cDNA was confirmed by DNA sequence analyses using 7 primer pairs. The cDNA was sequenced in its entirety after transfer into the yeast vector and no other modifications due to mutagenesis were identified.

2.3. Electrophysiology

CHO-K1 cells (RIKEN BRC Cell Bank, Tsukuba, Japan) were cultured in Ham's F-12 medium (HyClone, Logan, UT) supplemented with 10% fetal bovine serum and 1% penicillin-streptomycin in an incubator with a humidified atmosphere of 5% CO_2 at 37°C. CHO-K1 cells were transiently co-transfected with the following combinations of vectors: *KCNH2* WT cDNA (1 μg) plus green fluorescent protein (GFP) in pCGI vector (1 μg), *KCNH2* WT (1μg) plus *KCR1* WT (1μg), *KCNH2* WT (1μg) plus *KCR1* E33D (1 μg), or *KCNH2* WT (1 μg) plus *KCR1* WT (0.5 μg) plus *KCR1* E33D (0.5 μg), using FuGENE 6 Transfection Reagent (Roche, Indianapolis, IN). Cells displaying green fluorescence 48–72 hours after transfection were subjected to electrophysiological analysis.

Membrane currents were studied using the whole cell patch clamp technique with an amplifier, Axopatch-200B (Axon Instruments, Foster City, CA), at room temperature (23–25 °C). Electrode resistances ranged from 3 to 5 MΩ when filled by pipette with an intracellular solution containing: 110 mM KCl, 5 mM K_2ATP, 2 mM $MgCl_2$, 10 mM HEPES, and 5 mM K_4BAPTA at pH 7.2. During recording, the bath solution contained 140 mM NaCl, 5.4 XCl mM (X = sum of K^+ and *N*-methyl-D-glucamine$^+$ [NMDG]), 2 mM $CaCl_2$, 1.0 mM $MgCl_2$, 10 mM HEPES, and 10 mM glucose, adjusted to pH 7.4 with NaOH. Data acquisition and analysis were performed by a Digidata 1321 A/D converter and pCLAMP8.2 software (Axon Instruments, Foster City, CA).

All pulse protocols are described in the figures and figure legends; the holding potential in all cases was −80 mV. Voltage clamp command pulses were generated and patch clamp data were acquired using pCLAMP8 software (version 8.2, Axon Instruments). Data analysis was carried out using Clampfit (version 8.2, Axon Instruments).

Dofetilide was provided by Pfizer Global Research and Development (Sandwich, UK), and quinidine and D,L-sotalol were purchased from Sigma-Aldrich (St. Louis, MO). After I_{KCNH2} was recorded under control conditions, each drug was added to the bath solution at the indicated concentrations, followed by repetitive depolarizing pulses to +20 mV (2 s) from a holding potential of −80 mV (6 s) and hyperpolarizing pulses to −50 mV (2 s).

All values are expressed as mean ± standard error of the mean (SEM). Differences among these values were evaluated using an analysis of variance (ANOVA) and the unpaired Student's *t*-test where appropriate. A P value of <0.05 was considered to be significant.

2.4. Yeast transformation and Western blot analysis

The method for culturing and transformation of yeast was as described previously [13,18,19]. Equal numbers of yeast cells were inoculated into SD/-ura media plus 1 M Sorbitol and grown for 40 hours to a total density of 2.7×0^7 cells before transformation. *KCR1* WT, *KCR1* E33D or *ALG10* cDNAs were inserted into the pGPD426 vector and the vectors containing these cDNAs or pGPD426 empty vector (control), were transfected into the Alg10-deficient *wbp1-2/alg10* yeast strain YG649. As controls, the WT yeast strain SS328 and untransformed YG649 controls were grown in SD/-ura plus uracil and 1 M Sorbitol and processed in parallel. After transformation, the cells were grown on agar plates containing appropriate selection medium; individual colonies were picked from the plates and grown for 40 hours at 30 °C; the SS328 and untransformed YG649 controls were grown for 18 hours until comparable cell densities were reached, measured by $O.D._{600}$. Protein extracts from yeast cells were prepared for Western blot analysis as described previously [13].

3. Results

3.1. Molecular genetic analyses and clinical characteristics of a patient with a variant of KCR1

Genetic analysis revealed a novel variant of *KCR1* at amino acid position 33 (E33D) in a patient with ventricular fibrillation and QT prolongation (Fig. 1A, Table 1). We did not find this variant of *KCR1* in 200 healthy control individuals or any other mutation in this patient in all exons of *KCNQ1*, *KCNH2*, *SCN5A*, *KCNE1*, and *KCNE2*. However, we identified three mutations in *KCNH2* in three other patients: M124T and 527 ins C (R176fsX331) both in the N-terminus, and H492Y in the S2/S3 region (Table 1). In total, 4 out of 14 patients with aLQTS (29%) carried gene mutations. We also identified four polymorphisms: *KCNQ1* G643S, *SCN5A* H558R, *SCN5A* R1193Q, and *KCNE1* D85N (Table 1).

The patient with *KCR1* E33D was a 70-year-old man whose mother had died suddenly of unexplained causes. The patient had been treated with manidipine, kallidinogenase and bezafibrate for hypertension and hyperlipidemia since age 65. He suddenly fell unconscious in a restaurant and was found to have ventricular fibrillation by the emergency crew (Fig. 1B). After prompt defibrillation, he was brought to a hospital by ambulance. Blood chemistry results in the emergency room indicated hypokalemia (3.1 mEq/l). The ECGs which were recorded after admission indicated prolonged QTc (Fig. 1C). Metoprolol 60 mg and mexiletine 300 mg were initiated on the

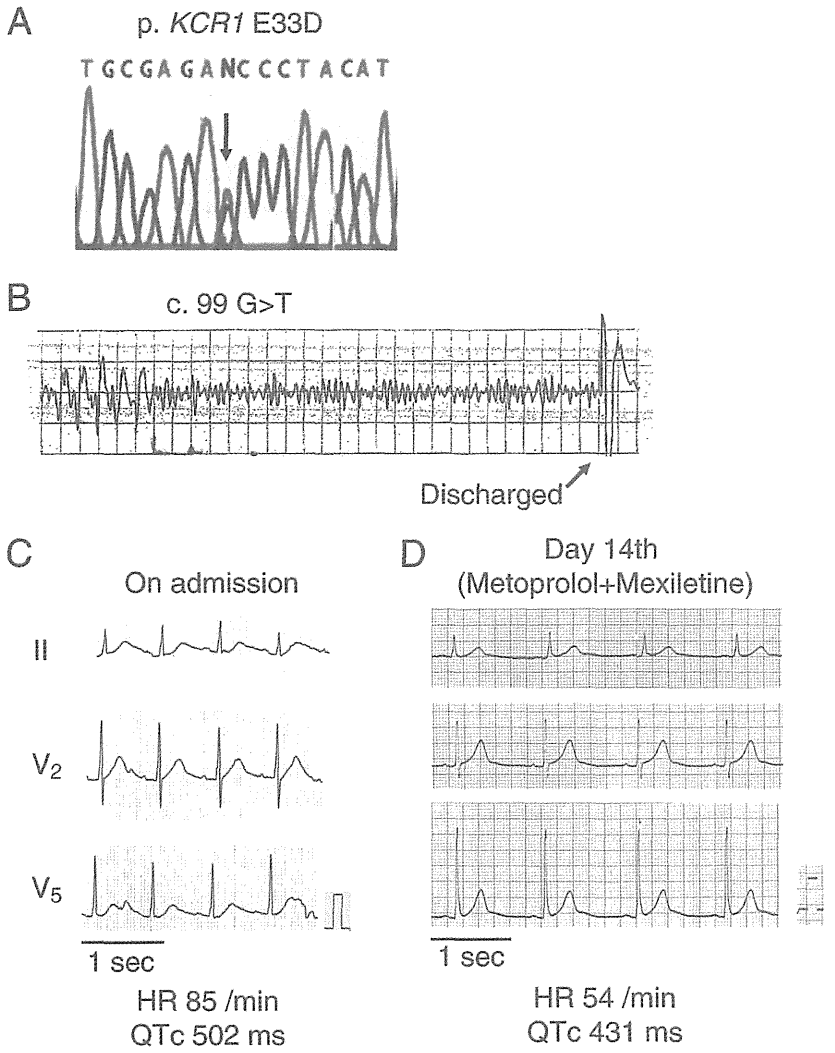

Fig. 1. Genetic analysis and electrocardiograms. (A) DNA sequence of *KCR1* showing the base sequence around the coding region of amino acid residue 33 in the patient with ventricular fibrillation and significant QT prolongation. (B) Electrocardiographic tracing during cardiopulmonary arrest. ECG shows ventricular fibrillation and discharge waveform by defibrillator. (C) and (D) ECGs recorded during hospital stay. ECG on admission shows prolonged QTc interval of 502 ms (C). In contrast, ECGs at day 14 after initiation of metoprolol and mexiletine show a normalized QTc interval (D).

Table 1
Mutations and polymorphisms identified in this study.

Gene	Nucleotide Change	Amino acid Change
Mutations		
KCR1	G99T	E33D
KCNH2	T371C	M124T
KCNH2	527 ins C	R176fsX331
KCNH2	C1474T	H492Y
Polymorphisms		
KCNQ1	G1927A	G643S
SCN5A	A1673G	H558R
SCN5A	G3578A	R1193Q
KCNE1	G253A	D85N

second hospital day, and an ECG on his 14th day of hospitalization showed that the QT interval had normalized (QTc 431 ms) (Fig. 1D).

3.2. Electrophysiological findings of KCNH2 channels co-expressed with KCR1 E33D

We previously reported that KCR1 had no effect on the activation gating or voltage dependence of inactivation [12]. Here, we evaluated the effect of the KCR1 E33D variant on KCNH2 channel activity. Fig. 2A shows representative current traces recorded in CHO cells expressing KCNH2 WT alone, KCNH2 WT + KCR1 WT, or KCNH2 WT + KCR1 E33D. Fig. 2B shows the current–voltage relationship for the peak activating currents, which was similar in all three conditions. The amplitude of the tail currents was plotted as a function of the test potential and the curve was fitted to a Boltzmann function. The voltage at which the tail current was half activated ($V_{1/2}$) was 4.35 ± 1.8 mV for KCNH2 WT alone (n = 14), 1.0 ± 1.8 mV for KCNH2 WT + KCR1 WT (n = 16), and 4.0 ± 1.6 mV for KCNH2 WT + KCR1 E33D (n = 16, P = NS compared with KCNH2 WT

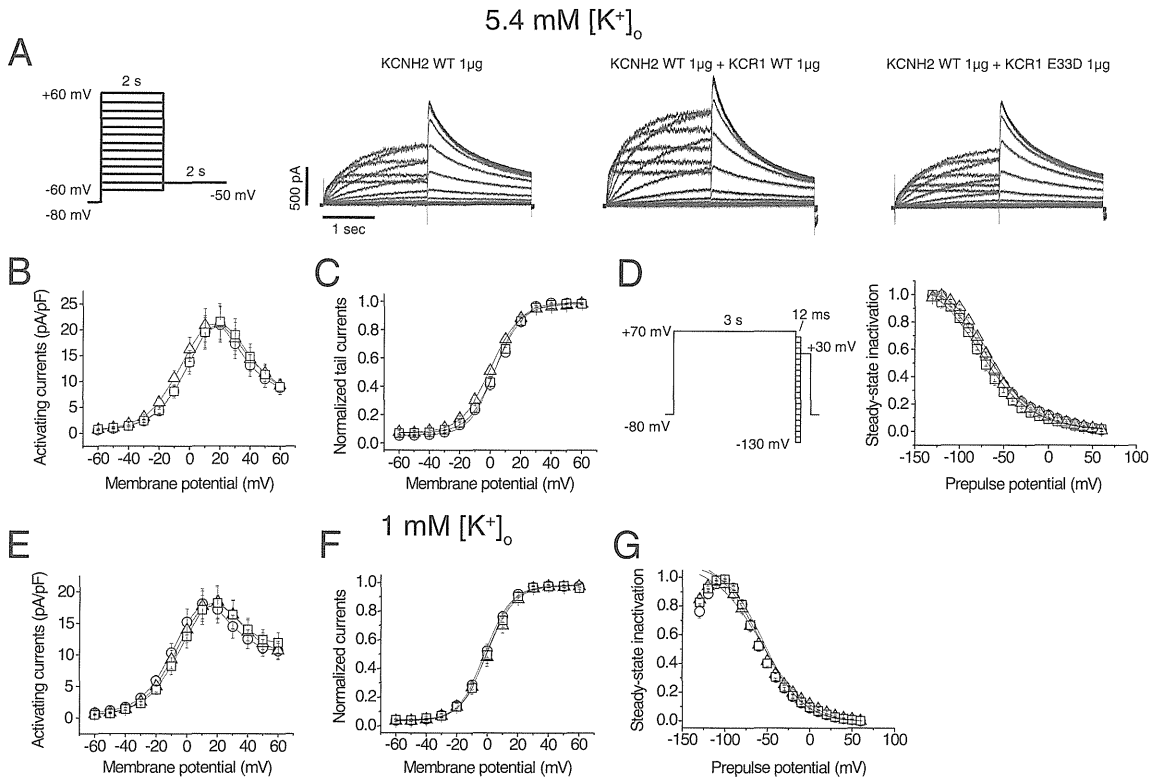

Fig. 2. Functional characterization of KCNH2 channels co-expressed with KCR1 E33D at varying $[K^+]_o$. (A) The activation voltage-clamp protocol (left). Representative currents expressed in CHO-K1 cells at 5.4 mM $[K^+]_o$, transfected with 1 μg *KCNH2* WT alone, 1 μg *KCNH2* WT plus *KCR1* WT, and 1 μg *KCNH2* WT plus 1 μg *KCR1* E33D variant. (B) *I–V* relationships for the peak currents in CHO-K1 cells at 5.4 mM $[K^+]_o$. *N* ranged from 14 to 16. (C) Normalized *I–V* relationships for mean amplitudes of tail currents at 5.4 mM $[K^+]_o$ in 14–16 experiments. (D) Voltage dependence of inactivation determined by a three-step protocol (left). Current amplitude at test potential was normalized and plotted against prepulse potentials. Normalized steady-state inactivation curves of expressed currents in CHO-K1 cells at 5.4 mM $[K^+]_o$ in 4–5 experiments. (E) *I–V* relationships for the peak currents in CHO-K1 cells at 1.0 mM $[K^+]_o$. *N* ranged from 15 to 17. (F) Normalized *I–V* relationships for mean amplitudes of tail currents at 1.0 mM $[K^+]_o$ in 13–16 experiments. (G) Normalized steady-state inactivation curves of expressed currents in CHO-K1 cells at 1.0 mM $[K^+]_o$ in 9–10 experiments. ○, *KCNH2* WT 1 μg; △, *KCNH2* WT 1 μg + *KCR1* WT 1 μg; □, *KCNH2* WT 1 μg + *KCR1* E33D 1 μg.

alone), indicating that KCR1 E33D did not affect the voltage dependence of activation of the KCNH2 WT channel (Fig. 2C). The voltage-dependent distribution of channels between the open and inactivated states was also examined using a 3-pulse clamp protocol (Fig. 2D). The peak tail current amplitude was measured in the final step to +30 mV and was plotted as a function of the preceding test potential. The $V_{1/2}$ for the voltage dependence of steady-state channel availability was −74.5 ± 7.8 mV ($n=5$) for KCNH2 WT alone, −70.0 ± 2.6 mV ($n=5$) for KCNH2 WT + KCR1 WT, and, −75.2 ± 4.1 mV ($n=4$) for KCNH2 WT + KCR1 E33D, indicating that the E33D variant did not affect the voltage dependence of steady-state inactivation.

Hypokalemia is a recognized risk factor for the LQTS, and because the index patient was slightly hypokalemic at the time of emergency room admission, it was important to ascertain the influence of extracellular K^+ concentration ($[K^+]_o$) in this paradigm [20]. We therefore repeated the same experiments in low $[K^+]_o$(1 mM). The results are shown in Fig. 2E–G. Fig. 2E shows the current–voltage relationships for activating peak currents during depolarizing pulses in 1 mM $[K^+]_o$. The voltage at which the tail current was half activated ($V_{1/2}$) was -0.52 ± 1.8 mV for KCNH2 WT alone (n = 16), 1.3 ± 2.4 mV for KCNH2 WT + KCR1 WT ($n=15$), and 1.1 ± 2.1 mV for KCNH2 WT + KCR1 E33D ($n=13$, P = NS compared with KCNH2 WT alone), (Fig. 2F). The $V_{1/2}$ for the voltage dependence of steady-state channel availability (Fig. 2G) was −54.8 ± 3.4 mV ($n=9$) for KCNH2 WT, −55.7 ± 3.8 mV ($n=10$) for KCNH2 WT + KCR1 WT, and, −55.2 ± 2.4 mV ($n=10$) for KCNH2 WT + KCR1 E33D. The fast and slow deactivation time constants of tail currents in 1 mM $[K^+]_o$ measured after a 2 sec depolarizing step to +20 mV and repolarization to potentials between −40 and −80 mV were comparable in cells transfected with KCNH2 WT alone ($n=15$), KCNH2 WT + KCR1 ($n=13$), and WT KCNH2 WT + KCR1 E33D ($n=12$) (data not shown). These results show that varying $[K^+]_o$ does not significantly alter the response of basal KCNH2 current to KCR1 WT or E33D.

3.3. Unlike KCR1 WT, E33D does not modulate sensitivity of I_{KCNH2} to channel blockers

We next evaluated whether the KCR1 E33D variant modulated drug sensitivity of the I_{KCNH2} current (Fig. 3). Representative traces of the KCNH2 WT tail currents recorded at −50 mV are shown in Fig. 3A. As reported previously, co-expression of KCR1 WT with KCNH2 WT protected I_{KCNH2} from the onset of inhibition by dofetilide. In contrast, co-expressing the E33D variant with KCNH2 WT had no significant effects on response to dofetilide (Fig. 3A and B). Following 100 pulses applied every 10 sec after application of 50 nM dofetilide in 5.4 mM $[K^+]_o$, 72 ± 4% ($n=13$) of the KCNH2 WT + KCR1 WT current remained, whereas only 51 ± 4% ($n=14$) of the KCNH2 WT + KCR1 E33D current remained ($P<0.05$ vs. KCNH2 WT + KCR1 WT) (Fig. 3B and D). The amount of inhibition of the KCNH2 WT + KCR1 E33D current was comparable to that of KCNH2 WT alone (53 ± 4%, $n=11$) (Fig. 3B and D). We estimated the IC_{50} for dofetilide to be 67 nM in the presence of the KCR1 E33D variant vs.

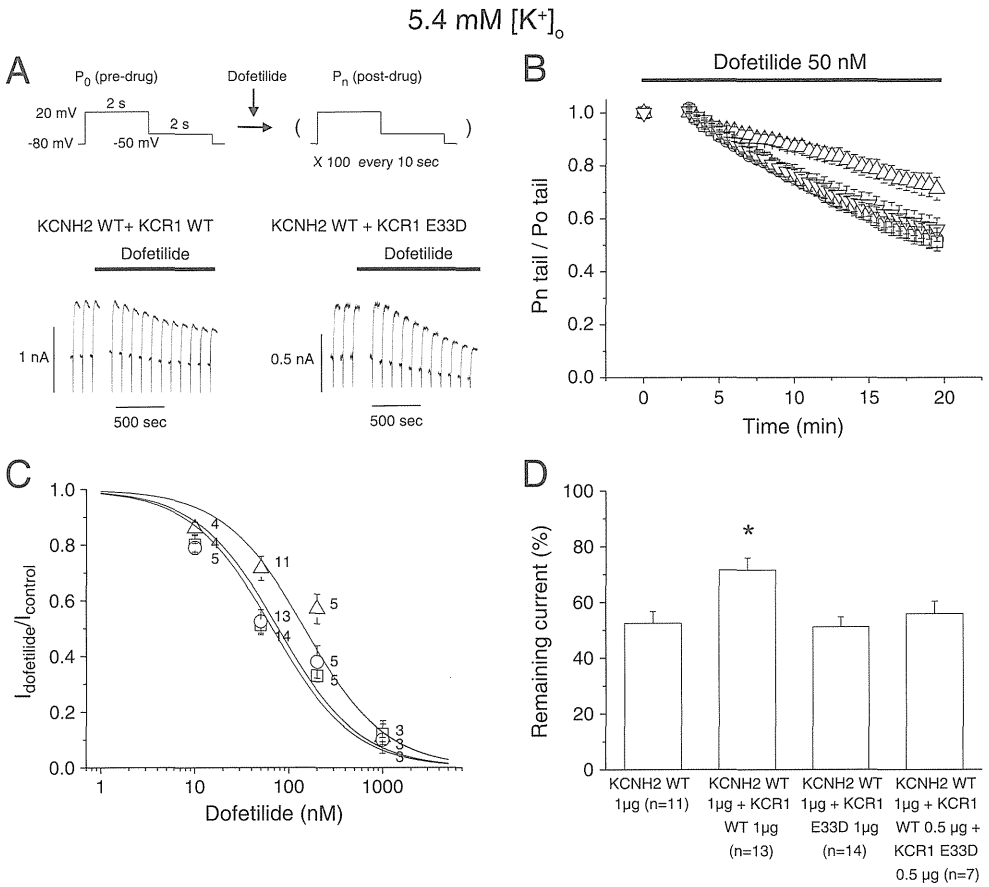

Fig. 3. Effects of KCR1 WT and E33D on dofetilide inhibition of KCNH2 current in CHO-K1 cells at 5.4 mM $[K^+]_o$. (A) Representative currents for KCNH2 WT plus KCR1 WT (bottom, left), and KCNH2 WT plus KCR1 E33D (bottom, right) during repetitive depolarizing pulses (top) in the presence of dofetilide. (B) Relative peak tail currents during repetitive pulses in the presence of dofetilide. *N* ranged from7 to 14. (C) Concentration dependence of blockade. Mean data were fitted to a logistic expression $(1/1+\{[D]/IC50\}^n)$, where [D] is dofetilide concentration and *n* is the Hill coefficient. (D) Percentage of outward current remaining after 100 pulses applied every 10 sec of 50 nM dofetilide perfusion. *$P<0.05$ versus KCNH2 WT, KCNH2 WT + KCR1 E33D, and KCNH2 WT + KCR1 E33D + KCR1 WT. ○, *KCNH2* WT 1 μg; △, *KCNH2* WT 1 μg + *KCR1* WT 1 μg; □, *KCNH2* WT 1 μg + *KCR1* E33D 1 μg; ▽, *KCNH2* WT 1 μg + *KCR1* WT 0.5 μg + *KCR1* E33D 0.5 μg.

146 nM in the presence of KCR1 WT (Fig. 3C). The IC_{50} of E33D was similar to that of KCNH2 WT alone (76 nM).

Because the patient with KCR1 E33D was heterozygotic for the mutation, we evaluated the effects of co-expressing WT and KCR1 variant on dofetilide sensitivity. Unlike KCR1 WT alone, co-expressing KCNH2 with KCR1 WT and E33D enhanced the drug blockade of I_{KCNH2} (Fig. 3B). Fig. 3D shows current remaining after 100 pulses applied every 10 sec after application of 50 nM dofetilide. The remaining current of KCNH2 WT + KCR1 WT + KCR1 E33D was 56 ± 5% ($n=7$), which was similar to that of KCNH2 WT alone, and significantly smaller than that of KCNH2 WT + KCR1 WT ($P<0.05$).

Fig. 4A plots the development of dofetilide blockade in 1 mM $[K^+]_o$ during a train of depolarizing pulses. Similar to the development of dofetilide blockade in 5.4 mM $[K^+]_o$ (Fig. 3), co-expressing KCNH2 WT and KCR1 WT slowed drug blockade of I_{KCNH2} compared to expressing KCNH2 WT alone or co-expressing KCNH2 WT and KCR1 E33D (Fig. 4A). The effect of co-expression of KCR1 WT and E33D on dofetilide blockade of I_{KCNH2} was intermediate between KCR1 WT alone and E33D alone (Fig. 4A). Fig. 4B shows the current remaining after 100 pulses after application of 50 nM dofetilide in 1 mM $[K^+]_o$. The remaining current of the KCNH2 WT + KCR1 E33D channel was 39 ± 5% ($n=8$), which was similar to that of the KCNH2 WT channel (37 ± 6%, $n=7$), and was significantly smaller than that of the KCNH2 WT + KCR1 WT channel (57 ± 4%, $n=7$, $P<0.05$). The amount of inhibition of the KCNH2 WT + KCR1 WT + KCR1 E33D current was 47 ± 3% ($n=7$), which was not significantly smaller than that of the KCNH2 WT + KCR1 WT current ($P<0.1$). In addition, the remaining current of the KCNH2 WT + KCR1 E33D channel after application of 50 nM dofetilide in 1 mM $[K^+]_o$ was significantly smaller than that in 5.4 mM $[K^+]_o$ (39 ± 5% versus 56 ± 5%, $P<0.05$). Thus, in low $[K^+]_o$, the same general effects of KCR1 WT and KCR1 E33D were observed, although overall levels of current remaining were smaller in 1 mM than in 5.4 mM $[K^+]_o$.

To determine if the effect of the KCR1 E33D variant can be generalized, we studied the effect of KCR1 on I_{KCNH2} blockade by quinidine and D,L-sotalol. Fig. 5A plots the development of quinidine blockade in the standard bath solution during repetitive depolarizing pulses. Quinidine at 2 μM produced rapid blockade, reaching equilibrium level of I_{KCNH2} inhibition within the first few test pulses. Contrary to KCR1 WT, KCR1 E33D did not reduce the extent of quinidine blockade (Fig. 5A and B); by the second pulse, the remaining current of the KCNH2 WT + KCR1 E33D channel was 56 ± 3% ($n=8$), which was similar to that of the KCNH2 WT channel (52 ± 3%, $n=7$) and that of the KCNH2 WT + KCR1 WT + KCR1 E33D channel (58 ± 4%, $n=10$), and was significantly smaller than that of the KCNH2 WT + KCR1 WT channel (73 ± 4%, $n=8$, $P<0.05$ vs. the

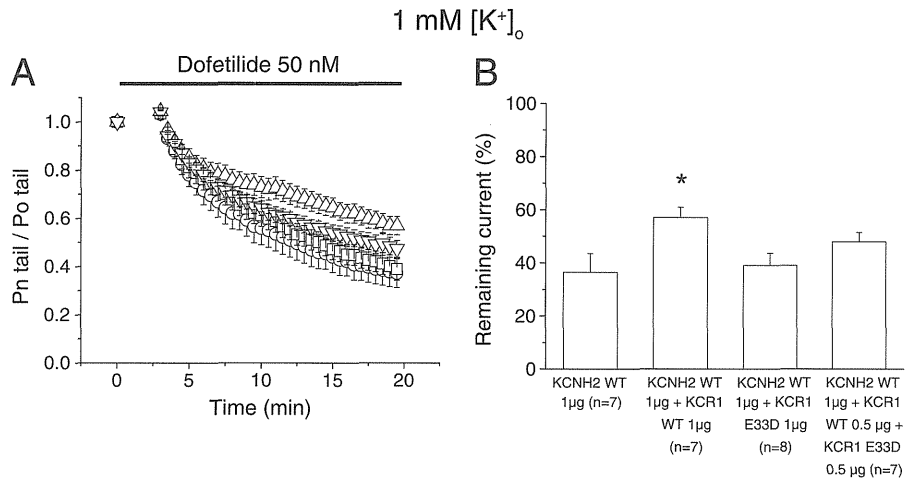

Fig. 4. Time-dependent blockade of KCNH2 current by dofetilide in low $[K^+]_o$. (A) Relative peak tail currents during repetitive pulses in the presence of 50 nM dofetilide for KCNH2 WT alone (○, $n=6$), KCNH2 WT plus KCR1 WT (△, $n=7$), KCNH2 WT plus KCR1 E33D (□, $n=8$), and KCNH2 WT plus KCR1 WT plus KCR1 E33D (▽, $n=7$). $[K^+]_o$ was 1.0 mM in these experiments. (B) Percentage of outward current remaining after 100 pulses applied every 10 sec of 50 nM dofetilide perfusion. *$P<0.05$ versus KCNH2 WT and KCNH2 WT plus KCR1 E33D.

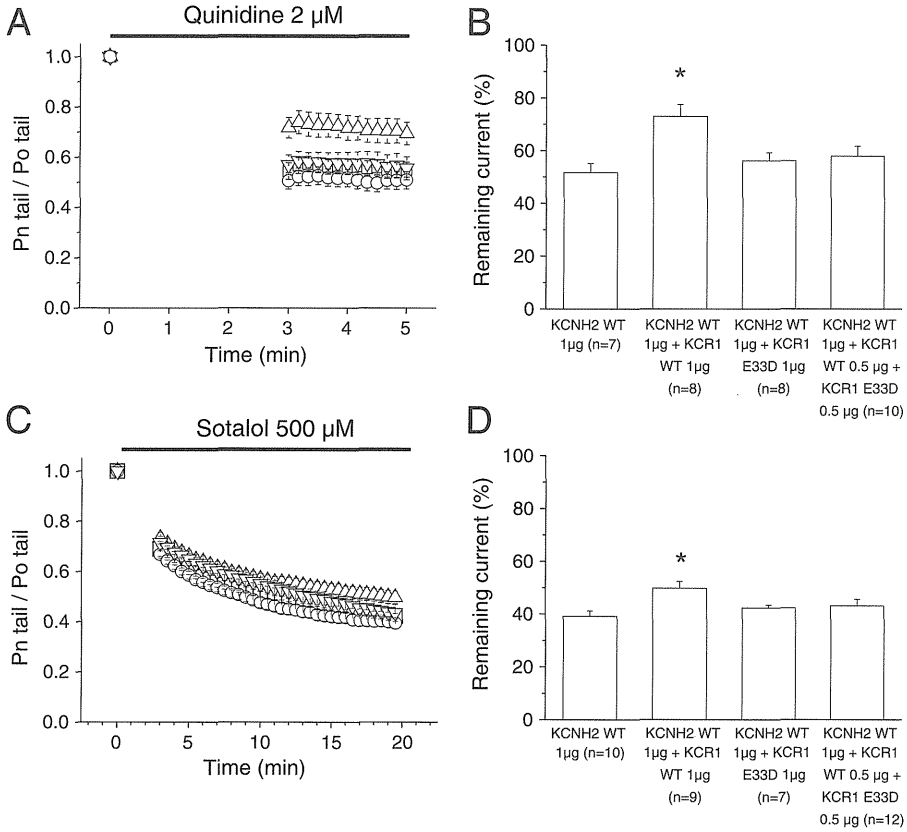

Fig. 5. Time-dependent blockade of KCNH2 current by quinidine and D,L-sotalol in the standard bath solution (5.4 mM $[K^+]_o$) (A) Relative peak tail currents during repetitive pulses in the presence of 2 μM quinidine. N ranged from 7 to 10. (B) Percentage of outward current remaining after 100 pulses applied every 10 sec of 2 μM quinidine perfusion. *$P<0.05$ versus KCNH2 WT and KCNH2 WT plus KCR1 E33D. (C) Relative peak tail currents during repetitive pulses in the presence of 500 μM D,L-sotalol. *N* ranged from 7 to 12. (D) Percentage of outward current remaining after 100 pulses applied every 10 sec of 500 μM sotalol perfusion. *$P<0.05$ versus KCNH2 WT and KCNH2 WT plus KCR1 E33D. ○, *KCNH2* WT 1 μg; △, *KCNH2* WT 1 μg + *KCR1* WT 1 μg; □, *KCNH2* WT 1 μg + *KCR1* E33D 1 μg; ▽, *KCNH2* WT 1 μg + *KCR1* WT 0.5 μg + *KCR1* E33D 0.5 μg.

KCNH2 WT + KCR1 E33D channel). Fig. 5C shows the development of sotalol blockade in the standard bath solution. D,L-sotalol blockade developed rapidly and reached an equilibrium level of I_{KCNH2} inhibition over minutes. I_{KCNH2} remaining after 100 pulses of 500 μM D,L-sotalol exposure was 42 ± 1% of the predrug control for the KCNH2 WT + KCR1 E33D channel ($n=7$), which was comparable to 39 ± 2% for the KCNH2 WT channel ($n=10$), but 50 ± 3% for the KCNH2 WT + KCR1 WT channel ($n=9$) ($P<0.05$ vs. the KCNH2 WT + KCR1 E33D channel or vs. the KCNH2 WT channel) (Fig. 5C and D). The amount of inhibition of the KCNH2 WT + KCR1 WT + KCR1 E33D current was 43 ± 2% ($n=12$), which was not significantly smaller than that of the KCNH2 WT + KCR1 WT current ($P<0.1$).

3.4. Unlike WT, the E33D variant does not rescue a growth defect caused by alg10 deficiency in yeast and does not possess α-glucosyltransferase activity

The closest known homolog of *KCR1* is the yeast α-glucosyltransferase, *ALG10*. We previously demonstrated that the mammalian *KCR1* cDNA, when introduced into yeast, is able to rescue a growth defect in the alg10-deficient yeast strain YG649 [13]. Fig. 6 reiterates that this growth defect is complemented by transformation with a yeast vector expressing *ALG10* (Fig. 6A, Section 3) or *KCR1* WT (Fig. 6A, Section 4). In contrast, cells transformed with vector alone (Section 2) or with the E33D variant (Section 5) exhibited little or no growth in the same time period, indicating that the E33D variant has lost the ability to rescue the growth defect of the YG649 strain.

The α-glucosyltransferase activity of ALG10 and KCR1 can be conveniently measured by Western blot analysis of the ALG10 substrate carboxypeptidase Y (CPY), which is endogenous to yeast [13]. Since CPY contains four N-linked oligosaccharides, it migrates at five different positions on an SDS polyacrylamide gel [19]. We found that ALG10 and KCR1 are functional homologs in YG649, confirming our previous results [13]. They both produced the −1 and fully glycosylated forms of CPY (mCPY) (Fig. 6B, lanes 4 and 5, respectively), as well as the incompletely glycosylated forms that are preferentially produced by the alg10-deficient YG649 mutant (Fig. 6B, lanes 2 and 3). In contrast, the E33D variant (Fig. 6B, lane 6) did not produce the fully glycosylated form (mCPY), thus functioning at a level similar to YG649 transformed with vector alone (Fig. 6B, lane 3). This indicates that the E33D mutation results in a loss of KCR1-associated α- glucosyltransferase activity in yeast.

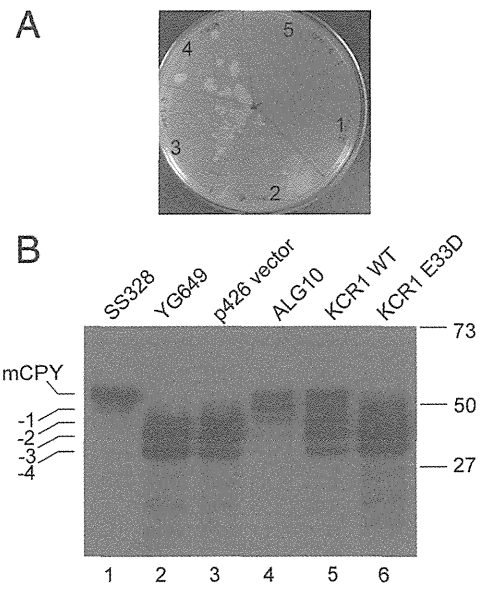

Fig. 6. Unlike KCR1 WT, KCR1 E33D fails to rescue the *alg10* defect in yeast. (A) The alg10-deficient yeast strain YG649 (*wbp1-2/alg10*) was either untransformed (1), or transformed with the E33D variant (5), empty vector (2), vector plus *KCR1* WT (4), vector plus *ALG10* (3), and plated on SD/-ura selective growth media. The vector carries a URA selection marker to facilitate identification of transformants. (B) Whole cell protein extracts were prepared from the transformed and control yeast strains and processed for Western blot analysis by electrophoresis on 10% SDS polyacrylamide gels. The gels were subjected to Western blot analysis using an anti-CPY antibody. Lane 1, SS328 (WT), the mature, fully glycosylated form of CPY (mCPY) is produced preferentially; lane 2, the YG649 *wbp1-2/alg10* mutant yeast strain mainly produces the incompletely glycosylated −4, −3, and −2 forms of CPY; lane 3, YG649 transformed with empty vector; lane 4, transformed with *ALG10*; lane 5, transformed with *KCR1* WT; lane 6, transformed with E33D variant of *KCR1*. Molecular mass markers are indicated on the right. The positions of the −4, −3, −2, −1 and mature glycosylated forms of CPY are indicated on the left. Three independent experiments produced comparable results.

4. Discussion

The aLQTS has many possible underlying causes, the most common of which are side effects from medications administered for unrelated conditions. Underlying structural heart disease is also a risk factor for the aLQTS [1]. Several reports have described the role of genetic variants in aLQTS [5–7,21,22]. Unrecognized congenital LQTS and its predisposing DNA polymorphisms were identified as risk factors for drug-induced TdP [1]. These genetic variants decreased or altered heterologously expressed currents or increased the drug sensitivity of I_{KCNH2} [5,7,21].

We have previously reported that KCR1 is expressed in human heart, modulates drug blockade of I_{KCNH2} through the cellular glycosylation pathway, and functions as an α-1,2 glucosyltransferase [12,13]. In control populations, basal levels of KCR1 expression in the heart provide a level of protection against inhibition of I_{Kr} by therapeutic agents. Indeed, polymorphisms in *KCR1* (I447V) exist that appear to improve the ability of KCR1 to prevent drug-induced LQTS [14]. In contrast, in this study, we showed that the KCR1 E33D did not protect KCNH2 from the effects of well-characterized KCNH2 inhibitors, including the class I antiarrhythmic quinidine, and the class III antiarrhythmics, dofetilide and sotalol (Figs. 3–5). The KCR1 E33D variant may enhance susceptibility to aLQTS by decreasing the biochemical activity of KCR1 (α-glucosyltransferase activity, see Fig. 6) and therefore lowering the ability of KCR1 to protect I_{Kr} from the effects of the drug. Because the patient with KCR1 E33D is heterozygotic for the variant, we evaluated the effect of co-expression of KCR1 WT and E33D on the dofetilide blockade of I_{KCNH2}. Co-expressing KCNH2 with KCR1 E33D and KCR1 WT to approximate the heterozygous condition enhanced the effects of dofetilide on the KCNH2 current, similar to expressing KCNH2 alone or co-expressing KCNH2 and KCR1 E33D (Figs. 3B, D, 4, and 5).

In a prior study using computational modeling, we showed that KCNH2 blockade, sufficient to evoke action potential prolongation and development of early after-depolarizations could be reversed by KCR1 effects on I_{KCNH2} [13]. The present study shows that the effects of dofetilide on the I_{KCNH2} current were not reduced by co-expression of KCR1 E33D alone or KCR1 WT and E33D. This suggests that KCR1 E33D may be proarrhythmic when normal KCNH2 function is diminished.

We further evaluated the effect of the variant versus WT KCR1 on KCNH2 currents at different potassium concentrations because the patient with KCR1 E33D was found to be hypokalemic at admission to a hospital. The remaining current of the KCNH2 WT + KCR1 E33D channel after application of 50 nM dofetilide in 1 mM $[K^+]_o$ was significantly smaller than that in 5.4 mM $[K^+]_o$ (Figs. 3 and 4). Lowering the extracellular potassium concentration decreases the magnitude of I_{Kr} and of outward KCNH2 K^+ currents [23,24]. Further, raising serum $[K^+]_o$ to the high normal range can normalize QT prolongation in some congenital long QT patients with KCNH2

mutations and in patients with acquired QT prolongation [25,26]. These effects run counter to what would be predicted by the Nernst equation because they are opposite to what is expected from a simple change in electrochemical driving force. Additionally, previous studies demonstrated that the I_{Kr} blocking properties of dofetilide were strikingly dependent on extracellular potassium [27]. The sensitivity of I_{Kr} to blocking drugs at low $[K^+]_o$ was significantly increased compared to that at high $[K^+]_o$ [27]. These findings may explain our observation that current levels were smaller overall at low $[K^+]_o$.

Furthermore, we also assessed the effect of the KCR1 E33D variant on KCNH2 blockade by anti-arrhythmic drugs other than dofetilide to determine whether the effect of the "loss of function" variant of *KCR1* is generalized. Blockade of the KCNH2 channel by dofetilide required channel activation and resulted in a time-dependent decline of the open channel current [28]. We selected quinidine and D,L-sotalol whose mode of action on KCNH2 channel is different from dofetilide. Quinidine exhibited a rapid onset of blockade, with steady-state achieved before the first few test pulses [29]. Meanwhile, the D,L-sotalol blockade of the KCNH2 channel was biphasic: a significant inhibition with the initial pulse and ready relaxation to equilibrium blockade with subsequent test pulses. Our findings show that KCR1 E33D significantly increased the sensitivity of I_{KCNH2} to both quinidine and D,L-sotalol as well as dofetilide, and may be associated with drug induced QT prolongation and tachyarrhythmia. We therefore speculate that reduced repolarization reserve due to enhanced I_{Kr} inhibition caused by a "loss of function" KCR1 variant (e.g. E33D) combined with the hypokalemic state may contribute to arrhythmia development, especially if a patient were to take an unrecognized I_{Kr} blocker [30].

In general, we expect that loss of function variants in *KCR1*, such as E33D, would increase the susceptibility of cardiac I_{Kr} to inhibition by KCNH2 inhibitors. The results from our study indicate that the E33D variant in *KCR1* leads to a loss of protection from blockade by the prototypical KCNH2 blockers in vitro, as well as loss of enzymatic α-glycosyltransferase function in a yeast expression system. This is the first report implicating a loss of function variant in *KCR1* in QT prolongation and ventricular fibrillation, although further studies are necessary to determine how diminished function of endogenous KCR1 in the heart can lead to increased arrhythmia susceptibility.

Funding Sources

This work was supported by a grant for cardiovascular disease research from the Japan Heart Foundation/Pfizer Japan Inc (to KH), and partially supported by the National Institutes of Health (RO1 HL69914 and HL090790 to SK).

Disclosures

None.

Acknowledgments

We thank Dr. Dan M. Roden for carefully reading our manuscript and providing helpful suggestions.

References

[1] Roden DM, Viswanathan PC. Genetics of acquired long QT syndrome. J Clin Invest 2005;115:2025–32.
[2] Donger C, Denjoy I, Berthet M, Neyroud N, Cruaud C, Bennaceur M, et al. KVLQT1 C-terminal missense mutation causes a forme fruste long-QT syndrome. Circulation 1997;96:2778–81.
[3] Makita N, Horie M, Nakamura T, Ai T, Sasaki K, Yokoi H, et al. Drug-induced long-QT syndrome associated with a subclinical SCN5A mutation. Circulation 2002;106:1269–74.
[4] Napolitano C, Schwartz PJ, Brown AM, Ronchetti E, Bianchi L, Pinnavaia A, et al. Evidence for a cardiac ion channel mutation underlying drug-induced QT prolongation and life-threatening arrhythmias. J Cardiovasc Electrophysiol 2000;11:691–6.
[5] Hayashi K, Shimizu M, Ino H, Yamaguchi M, Terai H, Hoshi N, et al. Probucol aggravates long QT syndrome associated with a novel missense mutation M124T in the N-terminus of HERG. Clin Sci (Lond) 2004;107:175–82.
[6] Paulussen AD, Gilissen RA, Armstrong M, Doevendans PA, Verhasselt P, Smeets HJ, et al. Genetic variations of KCNQ1, KCNH2, SCN5A, KCNE1, and KCNE2 in drug-induced long QT syndrome patients. J Mol Med 2004;82:182–8.
[7] Abbott GW, Sesti F, Splawski I, Buck ME, Lehmann MH, Timothy KW, et al. MiRP1 forms IKr potassium channels with HERG and is associated with cardiac arrhythmia. Cell 1999;97:175–87.
[8] Roti EC, Myers CD, Ayers RA, Boatman DE, Delfosse SA, Chan EK, et al. Interaction with GM130 during HERG ion channel trafficking. Disruption by type 2 congenital long QT syndrome mutations. Human Ether-a-go-go-Related Gene. J Biol Chem 2002;277:47779–85.
[9] McDonald TV, Yu Z, Ming Z, Palma E, Meyers MB, Wang KW, et al. A minK–HERG complex regulates the cardiac potassium current I(Kr). Nature 1997;388:289–92.
[10] Kagan A, Melman YF, Krumerman A, McDonald TV. 14-3-3 amplifies and prolongs adrenergic stimulation of HERG K + channel activity. EMBO J 2002;21:1889–98.
[11] Hoshi N, Takahashi H, Shahidullah M, Yokoyama S, Higashida H. KCR1, a membrane protein that facilitates functional expression of non-inactivating K + currents associates with rat EAG voltage-dependent K + channels. J Biol Chem 1998;273:23080–5.
[12] Kupershmidt S, Yang IC, Hayashi K, Wei J, Chanthaphaychith S, Petersen CI, et al. The IKr drug response is modulated by KCR1 in transfected cardiac and noncardiac cell lines. Faseb J 2003;17:2263–5.
[13] Nakajima T, Hayashi K, Viswanathan PC, Kim MY, Anghelescu M, Barksdale KA, et al. HERG is protected from pharmacological block by alpha-1, 2-glucosyl-transferase function. J Biol Chem 2007;282:5506–13.
[14] Petersen CI, McFarland TR, Stepanovic SZ, Yang P, Reiner DJ, Hayashi K, et al. In vivo identification of genes that modify ether-a-go-go-related gene activity in *Caenorhabditis elegans* may also affect human cardiac arrhythmia. Proc Natl Acad Sci U S A 2004;101:11773–8.
[15] Kupershmidt S, Snyders DJ, Raes A, Roden DM. A K + channel splice variant common in human heart lacks a C-terminal domain required for expression of rapidly activating delayed rectifier current. J Biol Chem 1998;273:27231–5.
[16] Mumberg D, Muller R, Funk M. Yeast vectors for the controlled expression of heterologous proteins in different genetic backgrounds. Gene 1995;156:119–22.
[17] Ho SN, Hunt HD, Horton RM, Pullen JK, Pease LR. Site-directed mutagenesis by overlap extension using the polymerase chain reaction. Gene 1989;77:51–9.
[18] Kupershmidt S, Yang T, Chanthaphaychith S, Wang Z, Towbin JA, Roden DM. Defective human Ether-a-go-go-related gene trafficking linked to an endoplasmic reticulum retention signal in the C terminus. J Biol Chem 2002;277:27442–8.
[19] Burda P, Aebi M. The ALG10 locus of *Saccharomyces cerevisiae* encodes the alpha-1, 2 glucosyltransferase of the endoplasmic reticulum: the terminal glucose of the lipid-linked oligosaccharide is required for efficient N-linked glycosylation. Glycobiology 1998;8:455–62.
[20] Roden DM. Taking the "idio" out of "idiosyncratic": predicting torsades de pointes. Pacing Clin Electrophysiol 1998;21:1029–34.
[21] Yang P, Kanki H, Drolet B, Yang T, Wei J, Viswanathan PC, et al. Allelic variants in long-QT disease genes in patients with drug-associated torsades de pointes. Circulation 2002;105:1943–8.
[22] Itoh H, Sakaguchi T, Ding WG, Watanabe E, Watanabe I, Nishio Y, et al. Latent genetic backgrounds and molecular pathogenesis in drug-induced long-QT syndrome. Circ Arrhythm Electrophysiol 2009;2:511–23.
[23] Sanguinetti MC, Jiang C, Curran ME, Keating MT. A mechanistic link between an inherited and an acquired cardiac arrhythmia: HERG encodes the IKr potassium channel. Cell 1995;81:299–307.
[24] Sanguinetti MC, Jurkiewicz NK. Role of external Ca2+ and K + in gating of cardiac delayed rectifier K + currents. Pflugers Arch 1992;420:180–6.
[25] Choy AM, Lang CC, Chomsky DM, Rayos GH, Wilson JR, Roden DM. Normalization of acquired QT prolongation in humans by intravenous potassium. Circulation 1997;96:2149–54.
[26] Compton SJ, Lux RL, Ramsey MR, Strelich KR, Sanguinetti MC, Green LS, et al. Genetically defined therapy of inherited long-QT syndrome. Correction of abnormal repolarization by potassium. Circulation 1996;94:1018–22.
[27] Yang T, Roden DM. Extracellular potassium modulation of drug block of IKr. Implications for torsade de pointes and reverse use-dependence. Circulation 1996;93:407–11.
[28] Snyders DJ, Chaudhary A. High affinity open channel block by dofetilide of HERG expressed in a human cell line. Mol Pharmacol 1996;49:949–55.
[29] Weerapura M, Nattel S, Chartier D, Caballero R, Hebert TE. A comparison of currents carried by HERG, with and without coexpression of MiRP1, and the native rapid delayed rectifier current. Is MiRP1 the missing link? J Physiol 2002;540:15–27.
[30] Roden DM. Long QT syndrome: reduced repolarization reserve and the genetic link. J Intern Med 2006;259:59–69.

The Journal of International Medical Research
2011; 39: 522 – 527

Expression Profiling of the Ephrin (*EFN*) and Eph Receptor (*EPH*) Family of Genes in Atherosclerosis-related Human Cells

A SAKAMOTO[1], Y SUGAMOTO[1], Y TOKUNAGA[1], T YOSHIMUTA[1], K HAYASHI[2], T KONNO[2], MA KAWASHIRI[2], Y TAKEDA[2] AND M YAMAGISHI[2]

[1]Division of Vascular Biology, National Cerebral and Cardiovascular Centre, Suita, Osaka, Japan; [2]Division of Cardiovascular Medicine, Kanazawa University Graduate School of Medicine, Kanazawa, Ishikawa, Japan

Ephrin B1 and its cognate receptor, Eph receptor B2, key regulators of embryogenesis, are expressed in human atherosclerotic plaque and inhibit adult human monocyte chemotaxis. Few data exist, however, regarding the gene expression profiles of the ephrin (*EFN*) and Eph receptor (*EPH*) family of genes in atherosclerosis-related human cells. Gene expression profiles were determined of all 21 members of this gene family in atherosclerosis-related cells by reverse transcription–polymerase chain reaction analysis. The following 17 members were detected in adult human peripheral blood monocytes: *EFNA1* and *EFNA3* – *EFNA5* (coding for ephrins A1 and A3 – A5); *EPHA1*, *EPHA2*, *EPHA4* – *EPHA6* and *EPHA8* (coding for Eph receptors A1, A2, A4 – A6 and A8); *EFNB1* and *EFNB2* (coding for ephrins B1 and B2); and *EPHB1* – *EPHB4* and *EPHB6* (coding for Eph receptors B1 – B4 and B6). THP-1 monocytic cells, Jurkat T cells and adult arterial endothelial cells also expressed multiple *EFN* and *EPH* genes. These results indicate that a wide variety of ephrins and Eph receptors might affect monocyte chemotaxis, contributing to the development of atherosclerosis. Their pathological significance requires further study.

KEY WORDS: ATHEROSCLEROSIS; INFLAMMATION; CELL MIGRATION; EPHRIN; EPH RECEPTOR; GENE EXPRESSION PROFILE

Introduction

In the development of atherosclerosis, monocytes transmigrate through the endothelium and differentiate into macrophages.[1,2] It was previously demonstrated that ephrin B1 cell signalling peptide and its cognate receptor, ephrin receptor B2 (EphB2), which are key regulators of embryogenesis and morphogenesis,[3,4] are expressed in atherosclerotic lesions, and that both ephrin B1 and EphB2 inhibit monocyte chemotaxis.[5] There are few data, however, on the gene expression profile of the ephrin (*EFN*) and Eph receptor (*EPH*) family of genes in atherosclerosis-related human cells. The present study, therefore, analysed the expression of all 21 members of the *EFN* and *EPH* gene family in adult human monocytes and related cells.

Materials and methods

This study was performed in accordance with the International Code of Medical Ethics of the World Medical Association (Declaration of Helsinki).

CELL PURIFICATION AND CULTURE

Mononuclear cells from venous blood of healthy adult volunteers were prepared using Lymphoprep™ (Axis-Shield, Oslo, Norway). Monocytes were enriched by counter-flow centrifugal elutriation (R5E elutriation system; Hitachi Koki, Ibaraki, Japan) as described previously.[5] THP-1 monocytic cells and Jurkat T cells were purchased from the American Type Culture Collection (ATCC, Rockville, MD, USA) and cultured in RPMI medium supplemented with 10% heat-inactivated fetal bovine serum at 37 °C in a 5% carbon dioxide atmosphere. Adult human coronary artery endothelial cells (HCAEC) were obtained from the Applied Cell Biology Research Institute (Kirkland, WA, USA) and maintained in CSC medium (Applied Cell Biology Research Institute) at 37 °C in a 5% carbon dioxide atmosphere. For experiments with HCAEC cells up to the third passage were used.

RNA ISOLATION AND RT–PCR TEMPLATE PREPARATION

Total RNA was isolated from the cells using Isogen reagent (Nippon Gene, Tokyo, Japan),[5–8] and was cleared of genomic DNA by the use of genomic DNA wipe-out buffer from the QuantiTect™ Reverse Transcription Kit (Qiagen, Hilden, Germany). Reverse transcription–polymerase chain reaction (RT–PCR) was used in the present study instead of a microarray[9] because of its specificity. Forward and reverse primers were designed for particular exons within each gene using human genomic DNA as the common positive control template. The exon–intron structures of all human *EFN* and *EPH* genes were identified through the Map Viewer Web site (http://www.ncbi.nlm.nih.gov/mapview/map_search.cgi). The primer sets used in this study are shown in Table 1. Ex Taq™ polymerase (TaKaRa, Tokyo, Japan) was used for PCR and the reaction mixture was assembled to a total volume of 10 µl as follows: 6.65 µl water, 1.0 µl 10 × Ex Taq™ buffer, 0.8 µl dNTP mixture (comprising 2.5 mM of each nucleotide), 1.0 µl forward and reverse primers (5 µM of each primer), 0.5 µl template and 0.05 µl Ex Taq™ polymerase. The PCR was carried out with pre-heating (94 °C for 2 min) and 30 or 35 cycles of amplification (94 °C for 20 s, 55 °C or 60 °C for 30 s and 72 °C for 40 s). DNA-cleared RNA without reverse transcription and human genomic DNA (50 nM; Clontech, Palo Alto, CA, USA) were used as negative and positive control templates, respectively. For all cell types, PCR was repeated three to five times and representative data are shown.

Results

VALIDATION OF RT–PCR CONDITIONS

Each primer set amplified a single PCR product from genomic DNA (Fig. 1, lane 3 in each column) and no product from the DNA-cleared RNA (Fig. 1, lane 2 in each column). Thus, the RT–PCR products were specific to the target genes and were derived from the synthesized cDNA. When expression of the genes coding for ephrin B1 (*EFNB1*) and EphB2 (*EPHB2*) were examined in human monocytes, THP-1 cells and HCAEC (Fig. 1), expression was consistent with our previous data obtained by RT–PCR using different primers and an immunofluorescence technique.[5] The present RT–PCR method was, therefore, reliable for analysis of the

Advance Publication by-J-STAGE

Circulation Journal
Official Journal of the Japanese Circulation Society
http://www.j-circ.or.jp

Age-Dependent Clinical and Genetic Characteristics in Japanese Patients With Arrhythmogenic Right Ventricular Cardiomyopathy/Dysplasia

Seiko Ohno, MD, PhD; Iori Nagaoka, MD, PhD; Megumi Fukuyama, MD; Hiromi Kimura, MD, PhD; Hideki Itoh, MD, PhD; Takeru Makiyama, MD, PhD; Akihiko Shimizu, MD, PhD; Minoru Horie, MD, PhD

Background: Arrhythmogenic right ventricular cardiomyopathy/dysplasia (ARVC/D) is a heart muscle disease caused by desmosomal gene mutations, and presents as ventricular tachycardia and sudden cardiac death. Although the mean age at onset or diagnosis of ARVC/D are reported to be around the 30–40 s, the age-dependent clinical and genetic differences remain unknown.

Methods and Results: A total of 35 consecutive Japanese probands (23 male) who were clinically diagnosed with ARVC/D were enrolled in the present study, and genetic analysis of *PKP2*, *DSP*, *DSG2*, and *DSC2* was done. The mean age at the first symptom and at diagnosis was 38.6±14.8 years and 40.5±17.7 years, respectively. Probands in whom the onset was cardiopulmonary arrest were significantly younger (22.3±15.3 years) than those with arrhythmia (41.1±13.2 years) or congestive heart failure (45.7±8.5 years). On genetic screening, 19 mutation carriers were identified. Although there was no age dependence for each gene mutation carrier, carriers with *PKP2* premature stop codon developed the disease at a significantly younger age than other mutation carriers.

Conclusions: The initial clinical manifestations in some young probands were very severe, and *PKP2* mutations with a premature stop codon would be associated with disease onset at a younger age.

Key Words: Arrhythmia; Cardiac arrest; Cardiomyopathy; Genes

Arrhythmogenic right ventricular cardiomyopathy/dysplasia (ARVC/D) is a disease characterized by right ventricular dysfunction and malignant arrhythmia.[1] Recent advances in molecular genetics have clarified the genetic background of ARVC/D. To date, 10 different genes have been reported to cause ARVC/D.[2–9] The majority of ARVC/D-causing genes encode desmosomal proteins: *PKP2*, encoding plakophilin 2; *DSP*, desmoplakin; *DSG2*, desmoglein 2; *DSC2*, desmocolin 2; and *JUP*, junctional plakoglobin. The most common gene variant identified in ARVC/D patients is reportedly *PKP2*, in approximately 25% of ARVC/D patients.[3]

In Japan, we first reported an ARVC/D patient with *PKP2* mutation,[10] and, recently, 4 of 8 ARVC/D patients were reported to have desmosomal gene mutations.[11] In other Asian countries, although *PKP2* mutations were identified only in China,[12–14] no other desmosomal gene mutation has been reported. Therefore, further examination of the ARVC/D etiology in Asian ethnicities is required.

Reportedly, ARVC/D patients become symptomatic at around 40 years old.[15,16] More recently, however, clinical features of pediatric ARVC/D patients with desmosomal gene mutations have been reported.[17] Most patients in that study were family members of those diagnosed with ARVC/D, and only patients with mutations were included. Moreover, there has been little discussion of sporadic cases in young patients, regarding the early detection or prevention of sudden death. The age-dependent clinical/genetic differences remain to be studied in terms of ARVC/D, including mutation-negative or sporadic cases.

In this study, we screened mutations in 4 desmosomal genes in 35 Japanese probands diagnosed with ARVC/D and then analyzed clinical and mutational characteristics, especially with regard to age.

Received November 21, 2012; revised manuscript received January 7, 2013; accepted January 29, 2013; released online March 20, 2013 Time for primary review: 13 days

Department of Cardiovascular and Respiratory Medicine, Shiga University of Medical Science, Otsu (S.O., I.N., M.F., H.K., H.I., M.H.); Department of Cardiovascular Medicine, Kyoto University Graduate School of Medicine, Kyoto (S.O., T.M.); and Faculty of Health Sciences, Yamaguchi University Graduate School of Medicine, Ube (A.S.), Japan

Mailing address: Minoru Horie, MD, PhD, Department of Cardiovascular and Respiratory Medicine, Shiga University of Medical Science, Seta-Tsukinowa-cho, Otsu 520-2192, Japan. E-mail: horie@belle.shiga-med.ac.jp

ISSN-1346-9843 doi:10.1253/circj.CJ-12-1446

Table 1. Subject Clinical Characteristics and Diagnosis

Family no.	Sex	Age at onset (years)	Age at diagnosis (years)	RV function and structure	Task force criteria					Diagnosis		
					Tissue	Repolarization	Depolarization/ Conduction	Arrhythmia	Family history	Major criteria	Minor criteria	Category
1	M	29	30	A			I	I	M	2	2	Definite
2	M	48	49	A	I			I		1	2	Definite
3	M	16	16	A			A	I	M	3	1	Definite
4	F	36	36	A			A	I		2	1	Definite
5	M	51	51		I		A	A		2	1	Definite
6	F	–	15	A		I		I	M	2	2	Definite
7	M	40	64	A	A		I			2	1	Definite
8	F	15	15	A				A	M	3	0	Definite
9	M	44	49	A		I		A	M	3	1	Definite
10	F	47	47	A		I		A	M	3	1	Definite
11	M	71	72	A			I	I	M	2	2	Definite
12	M	42	45	A		A		A		3	0	Definite
13	M	40	40	A			I	I	M	2	2	Definite
14	M	41	41	A	A		I	I	M	3	2	Definite
15	F	–	16					I	M	1	1	Borderline
16	M	5	5	A				A		2	0	Definite
17	M	17	17	A		A		I	M	3	1	Definite
18	M	34	38			A	I	I		1	2	Definite
19	F	25	25			A		I		1	1	Borderline
20	F	50	63		I			I		0	2	Possible
21	M	43	43	A				A		2	0	Definite
22	M	30	30	A			I			1	1	Borderline
23	M	26	32				A	I		1	1	Borderline
24	F	47	47	A			I	A		2	1	Definite
25	M	58	70	A				I	A	2	1	Definite
26	F	17	18				I	I		0	2	Possible
27	M	48	56	A				A	M	3	0	Definite
28	F	42	43		A	A		A	M	4	0	Definite
29	M	25	25	A		A	A	I	M	4	1	Definite
30	F	55	63	A		A		A		3	0	Definite
31	M	55	56			I	I	A	M	2	2	Definite
32	M	49	50	I			I	I	M	1	3	Definite
33	M	27	34			A		A	M	3	0	Definite
34	M	54	62	A			I	I	M	2	2	Definite
35	F	44	53	A			I	I	M	2	2	Definite

A, major criteria; I, minor criteria; M, mutation positive; RV, right ventricular.

Methods

Subjects

The subjects consisted of 35 probands (23 male) clinically diagnosed with or suspected to have ARVC/D from unrelated families, and 16 family members from 8 families. Each underwent detailed clinical and cardiovascular examinations for diagnosis, including an electrocardiogram (ECG), echocardiography, magnetic resonance imaging, and Holter ECG. Some patients underwent RV angiography, myocardial biopsy, and signal-averaged electrocardiography. They were classified into 3 diagnostic categories of ARVC/D: definite, probable, and possible according to the 2010 diagnostic criteria.[18] They were referred consecutively to either of the present laboratories for genetic evaluation. All subjects submitted written informed consent in accordance with the guidelines approved by each institutional review board.

Genotyping

Genomic DNA was isolated from venous blood lymphocytes, as previously described.[19] Using polymerase chain reaction analysis and direct DNA sequencing, we performed a comprehensive open reading frame/splice site mutational analysis of 4 major ARVC/D susceptibility genes: *PKP2*, encoding plakophilin 2; *DSP*, encoding desmoplakin; *DSG2*, encoding desmoglein 2; and *DSC2*, encoding desmocolin 2. The cDNA sequences of *PKP2*, *DSP*, *DSG2,* and *DSC2* were based on the GenBank reference sequences NM_004572.3, NM_004415.2, NM_001943.3, and NM_004949.3, respectively. We did not screen for *JUP* (encoding junction plakoglobin). In addition to desmosomal genes, we screened for *LMNA*[20] in the present probands, and identified a missense mutation in 1 patient. In this study, we excluded the patient with a *LMNA* mutation from the analysis. All new putative pathogenic variants were examined in 200 reference alleles derived from unrelated